4. Technologies of Anti-Tactical Ballistic Missile Systems

This chapter deals with the technologies which are presently used or could be used in the future, to perform the basic functions of defense systems against tactical ballistic missiles: Searching and detecting incoming missiles (4.1); tracking the targets, guiding interceptors, and triggering the interceptor warheads (4.2); and techniques to counter the incoming warheads (4.3). Description will begin with present or near-term technologies, i.e., ground-based anti-missiles with local radars, and then continue to future concepts including remarks on beam weapons in space. Technical data of, and concepts for, anti-tactical ballistic missile systems are presented in 4.4.

4.1 Search and Detection

Because at a possible target, tactical ballistic missiles could come from different directions (i.e., azimuth and elevation angles), a large solid angle has to be searched. Because of the high velocity of approaching missiles, detection has to take place early enough to allow anti-missiles to be launched in time to meet the incoming missiles, at a safe distance from the target. Spending limited amounts of radar energy over a large solid angle is inconsistent with achieving long detection distances; therefore, for classical anti-tactical ballistic missile systems with local radars, the radar parameters limit the detection distance. To avoid this limitation, other, mostly passive, means for search are being considered which would detect incoming missiles at longer distances, like satellite-based short-wave infrared detectors or aircraft-based long-wave infrared sensors.

4.1.1 Search by Radar

4.1.1.1 Radar Equation and Radar Range

Because radar power is spread over an area which increases as the square of the distance on both ways, the received radar power P_r varies strongly, namely by the inverse fourth power of the distance R of the reflecting object. The radar equation for a point target (i.e., the size of the object is smaller than the beamwidth) is

$$P_r = P_t \frac{G A_{eff} \sigma}{(4\pi)^2 R^4 F_L} \qquad (4\text{-}1)$$

Here P_t denotes the transmitter power. The effective antenna area A_{eff} can change with the angle between the beam and the antenna axis; σ, the so-called radar cross section, is a complicated function of the size, shape, and reflective properties of the object and of the radar wavelength λ. For a circular plane wave of constant irradiance at the antenna, diffraction

theory shows that the antenna gain G, the factor by which the maximum irradiance in the far field exceeds that of an isotropic spherical wave, is

$$G = 4 \pi A_{eff} / \lambda^2. \tag{4-2}$$

Losses F_L occur at different stages in the transmitter, during propagation through the atmosphere and in the receiver; a typical value is 5 to 10 (7 to 10 dB in logarithmic units).

Detection of reflected signals takes place in the presence of noise which arises in the receiver and potentially by clutter targets. Usually the noise is assumed to have a Gaussian amplitude distribution; if the reflexes from n consecutive radar pulses are integrated, the detection range R_{Det} of a radar system (i.e., the range below which pre-set limits for the probabilities of detection and of false alarms are kept), turns out to be [1]

$$R_{Det} = \left[\frac{P_t A_{eff}^2 \sigma n E_i(n)}{4 \pi \lambda^2 k T_0 B_n F_n (S/N)_1 F_L} \right]^{1/4}. \tag{4-3}$$

Here the product of the pulse number n and the integration efficiency $E_i(n)$ is about equal to n for $n \lesssim 10$ (in case of coherent detection, for all n) and lies between $\sqrt{n}$ and n for higher pulse numbers and incoherent detection. The product of Boltzmann's constant k and a standard temperature $T_0 = 290$ K, $k T_0 = 4.00 \cdot 10^{-21}$ Joule, together with the noise-equivalent bandwidth B_n, would give the noise power of an ideal receiver. The bandwidth B_n is approximately equal to the inverse of the radar pulse duration, τ. The noise figure F_n, usually about 3 (5 dB in logarithmic units), is the factor by which the noise of the real receiver exceeds that of an ideal one. Choices of the acceptable false-alarm rate and the necessary detection probability, give a value for the signal-to-noise ratio for detection using one pulse, $(S/N)_1$, which may vary between 10 and about 60 (10 to 18 dB).[2]

4.1.1.2 Radar Cross Sections

Scattering of radar signals is produced by diffraction and reflection at every part of the target. For a given object, the radar cross section is a function of the wavelength, the polarization, and the aspect angles between the beam and the object. It is high if the signal is reflected specularly on a part of the object. It can be reduced, if materials of little conductivity and shapes without sharp edges are used. The radar cross section can be calculated analytically only for the most simple shapes. E.g. for a conducting sphere, the cross section varies with the inverse fourth power of the wavelength as long as the wavelength is greater than 2π times the radius r (Rayleigh region); if the wavelength is smaller than about 1/5 of this value, the radar cross section is constant and equals $2 \pi r^2$, the geometrical cross section of the sphere (optical region); in the intermediate region, the radar cross section has resonances with a maximum value of 3.6 times the geometrical cross section (Mie region). Table 4-1 gives expressions for the radar cross sections for some simple shapes. For a cone-sphere (with a sharp tip), the nose-on cross section is at maximum $0.4 \lambda^2$, independent of the size and largely independent of the cone opening angle. A reentry vehicle formed like a cone-sphere with a rounded tip will have a nose-on radar cross section of about the base area if the wavelength is about 2π times the base radius. For smaller wavelengths, the cross section will be about $0.1 \lambda^2$. If the wavelength decreases below 2π times the nose radius r_n, nosetip scattering will dominate and the cross section will be

$$\sigma = \pi r_n^2, \tag{4-4}$$

Tab. 4-1 Theoretical expressions for the radar cross sections of simple shapes in the optical region (i.e., the radar wavelength is markedly smaller than the object size).[3] The incidence angle is chosen for maximum signal (normal incidence at some part of the shape).

Shape	Radar cross section
Corner cube retroreflector, side a	$12 \pi a^4 / \lambda^2$
Flat plate, sides a and b, normal incidence	$4 \pi a^2 b^2 / \lambda^2$
Cylinder, radius a, length b, normal incidence	$2 \pi a b^2 / \lambda$
Sphere, radius a	πa^2
Sharp cone, half opening angle α, σ contribution by nose, nose-on	$\lambda^2 \tan^4 \alpha / (16 \pi)$
Rounded cone, radius of nose a, σ contribution by nose, nose-on	πa^2

which can be very low if the nose tip is sharp. The tip radius r_n is mainly dictated by the requirement that the reentry heat, which is maximum here, can be tolerated (see (3-27) in 3.1.2.4). For reentry vehicles of intercontinental ballistic missiles, the nose radius is about 4 cm;[4] thus the radar cross section could be 0.005 m^2, if a spherical back side were provided (for a flat back, σ would approximate the base area, for a reentry vehicle of 0.6 m base diameter about 0.3 m^2). Since in (3-27) the heat power influx at the nose scales with the cube of the reentry velocity and the inverse square root of the nose radius, for equal ballistic coefficient β and reentry angle α, and material of equal thermal endurance, the allowed nose radius scales with the sixth power of the reentry velocity, and the cross section contribution by the nose even with the 12th power. Thus, for a tactical ballistic missile with a range of 2,000 km and a reentry velocity of 4 instead of 7 km/s, the nose radius could theoretically be 30 times smaller. The radar cross section would not, however, decrease by the square of this factor, because it would tend to the limit of a sharp cone-sphere, which is between 0.01 and 0.4 times the wavelength squared.[5] Using a typical factor of 0.1 and a typical radar wavelength of 0.05 m (frequency 6 GHz), the radar cross section could still be lowered to about 0.0003 m^2. The same limit would hold for reentry vehicles of tactical ballistic missiles of shorter ranges. Table 4-2 gives some typical values of radar cross sections.

Tab. 4-2 Typical values of radar cross sections at frequencies in the microwave region (radar wavelengths between 5 mm and 1 m).[6]

Object	Radar cross section in m^2
Theoretical reentry vehicle of tactical ballistic missile	0.0003
Theoretical ICBM reentry vehicle	0.005
Cylinder with ogive nose, length 1.3 m, diameter 15 cm, nose-on	0.02
Conventional, unmmanned winged missile	0.5
Small, single-engine aircraft	1
Large fighter	6
Large bomber or large jet airliner	40

Fig. 4-1 demonstrates the complex variation of the radar cross section with azimuth angle for an airplane. Very small changes of aspect angle can give rise to changes in the cross section, and thus in the radar signal, of up to two orders of magnitude. Fig. 4-2 shows the angular dependence of the cross section for simple shapes which can serve as models for ballistic missiles and their reentry vehicles. One sees that if the aspect angle changes from nose-on, the cross section normally does not increase before fairly large angles from the axis are reached (and, e.g., specular reflection at a line of the cone or cylinder becomes dominant). This means that for detection of tactical ballistic missiles or of their reentry vehicles from the general direction of the target, the nose-on radar cross section is appropriate.

In reality, conditions of observation are not constant. The radar cross section will fluctuate with the motion of the object or the beam, with changes in meteorological conditions and the like. Using mathematical models for the probability distributions of the cross section values, statistical analysis of the detection probability is normally performed according to four cases (first analyzed by Swerling). These differ by the echo amplitude distribution function and by the assumption of independent echo signal values from scan to scan or from pulse to pulse. Usually, Swerling case 1 is assumed (Rayleigh exponential distribution, constant amplitudes pulse-to-pulse). In most cases, an increase in signal-to-noise ratio is required for the same probability of detection.[7]

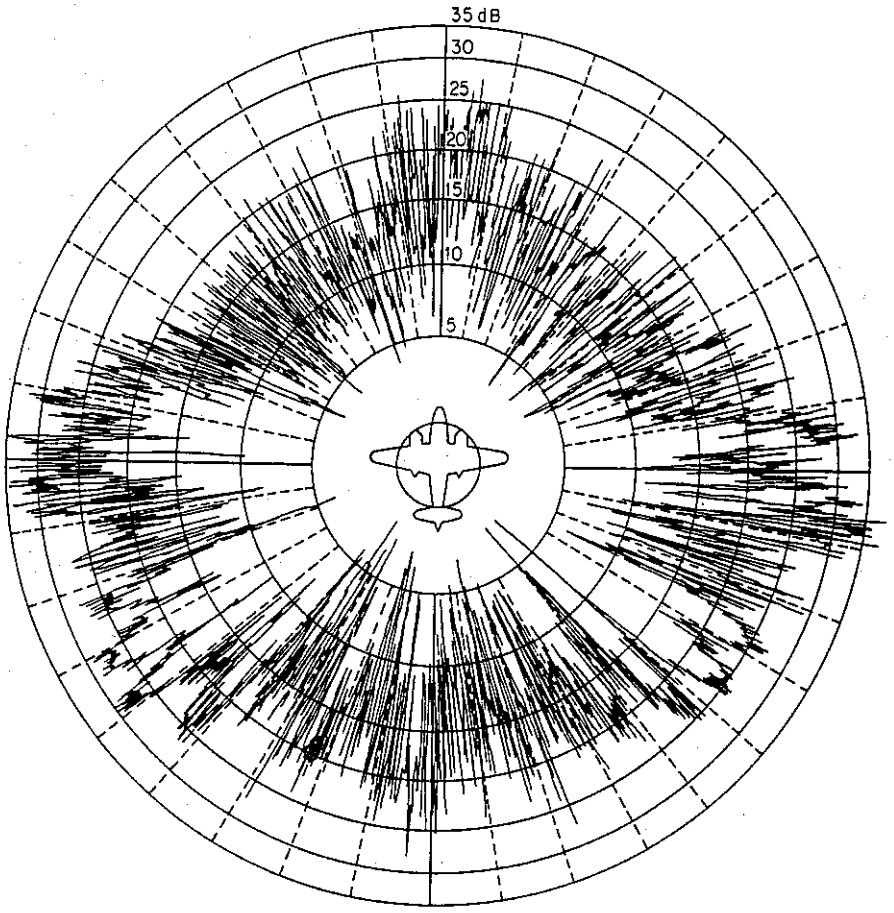

Fig. 4-1 Example of an experimental radar cross section as it varies with azimuth angle.[8] The target is a B-26 two-engine bomber, the wavelength is 0.1 meter. The cross section is given in relative logarithmic units.

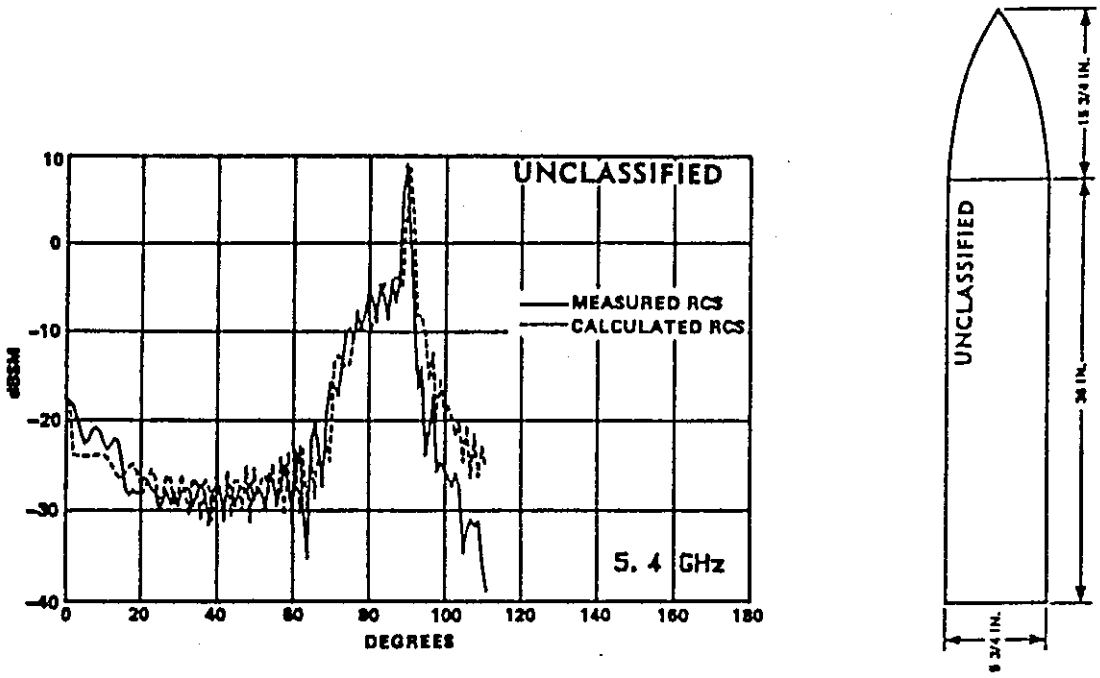

Fig. 4-2 Variation of the radar cross section in decibel referred to 1 m^2, with aspect angle Θ in degrees, for a cylinder with an ogive nose (length 1.3 m, diameter 0.15 m) at 5.4 GHz frequency (5.6 cm wavelength).[9]

4.1.1.3 Performance of Search Radars

An important parameter characterizing radars is the average power P_{av}. If pulses of duration τ are repeated with a pulse frequency f_p, it is given by

$$P_{av} = P_t \tau f_p \tag{4-5}$$

where P_t is the peak power of the pulse. A search radar has to cover a certain solid angle Ω; if the solid angle of the beam is ω, the number of different beam positions is Ω/ω. If during its slew, the beam hits a target for a dwell time T_d, then for uniform coverage the time required for the whole search solid angle, the frame time T_f, is

$$T_f = T_d \Omega / \omega. \tag{4-6}$$

In order to maximize the detection probability, all n radar pulses reflected during the dwell time are integrated, where n is given by

$$n = T_d f_p. \tag{4-7}$$

If the objects to be searched approach the radar with a radial velocity v, the distance Δ traveled during a frame time is

$$\Delta = v T_f. \tag{4-8}$$

In case of coherent integration, the integration efficiency $E_i(n)$ in (4-3) is 1. Remembering that $B_n = 1/\tau$, one can substitute the product $P_t \cdot n \cdot \tau$ in (4-3), the total energy transmitted during the dwell time, by $P_{av} \cdot T_d$. Further, one can use the fact that the antenna gain is

$$G = 4\pi / \omega, \tag{4-9}$$

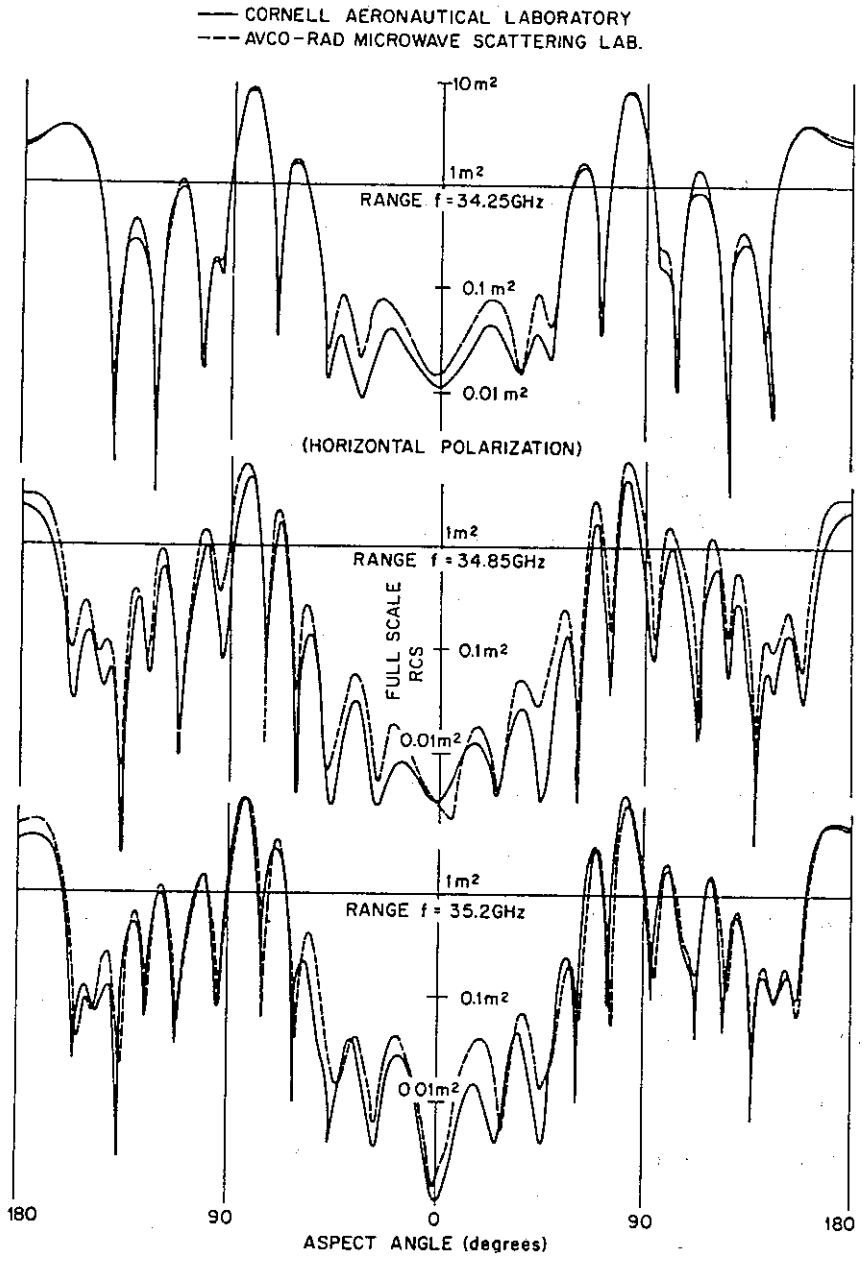

Fig. 4-3 Experimental radar cross section in m^2 versus aspect angle in degrees for a ballistic reentry nose cone of 1965, horizontal polarization, for frequencies around 35 GHz (wavelength 8.5 mm).[11]

substitute (4-6) solved for ω, and introduce Δ from (4-8). This yields an equation for the range R_0 where, for observation during one dwell time, a signal-to-noise ratio of 1 is achieved:[10]

$$R_0^4 = \frac{P_{av} A_{eff} \sigma}{4 \pi k T_0 F_n F_L \Omega v} \Delta = r_1^3 \Delta. \qquad (4\text{-}10)$$

The distance r_1, defined by the second equation of (4-10), does not depend on the radar wavelength or the pulse frequency. For non-coherent integration, a correction factor Q_i has to be applied for r_1:

$$r_1 = \left[\frac{P_{av} A_{eff}\, \sigma}{4\,\pi\, k\, T_0\, F_n\, F_L\, \Omega\, v}\right]^{1/3} Q_i. \qquad (4\text{-}11)$$

Q_i is 1 for a false alarm probability of 10^{-6} (i.e., 1 false alarm in 10^6 possible decision intervals of length $\tau = 1/B_n$), and integration over $n = 1$ pulse. Q_i decreases slowly with increasing pulse number and increasing false alarm number. Given the radar parameters: average power P_{av}, antenna area A_{eff}, noise factor F_n, loss factor F_L, and solid angle to be searched Ω, and given the cross section of the target σ as well as its radial velocity v, the quantity r_1 is fixed. For search optimization, one can then choose the frame time T_f and thus the distance Δ. Large frame times give long dwell times, with better detection probability during a single scan. On the other hand, if the target has not been detected during one scan, after one long frame time it may have approached far too much for the defense to react. For a search radar of a defense system, one is interested in maximizing the cumulative detection probability over several frame times. This quantity has a maximum, if the frame time varies in proportion to the quantity r_1;[12] in terms of the distance Δ traveled radially during one frame time,

$$\Delta = v\, T_f = \delta\, r_1, \qquad (4\text{-}12)$$

where the constant δ depends only on the target fluctuation characteristics and the chosen value of the cumulative detection probability. This means that the integration time T_d for each direction varies in proportion to the cube root of the power-aperture product. If this optimum search condition is fulfilled, then the detection range varies no longer with the fourth, but with the cube root of the power-aperture product. This seeming deviation from the fourth root scaling of (4-3) can be understood by realizing that the number n of pulses in (4-3) is not constant, but is varied in proportion to the cube root of the power-aperture product. (Note that for real search radars with constant pulse energy the detection distance is reported to depend on the 3.5th to 3.74th root of the power-aperture product.[13]) Numerical values for given detection probability and cross section fluctuation behaviour can be taken from Ref. 14; for typical conditions, the optimum ratio δ between the distance Δ and the value r_1 defined in (4-8) is 0.03 to 0.15. The search detection distance R_{DetS} is then proportional to r_1 too:

$$R_{DetS} = \rho\, r_1; \qquad (4\text{-}13)$$

the ratio ρ is between 0.1 and 0.2 for cumulative detection probabilities between 90 and 98%. Of course, different target characteristics (i.e., cross section and velocity values) lead to different optimum radar parameters; in designing a radar system and its operating modes, a compromise has to be taken. In any actual search of a given defense radar, the pulse and beam slew characteristics cannot be simultaneously optimized for detection of short-range ballistic missiles and intermediate range ones; neither is simultaneous optimized detection of ballistic missiles and aerodynamic vehicles possible. In order to use an estimate which is optimistic for the defense, however, only the respective optimum cases will be used in the following.

An example will give an indication of the optimum detection range: Assume a radar like that of the U.S. mobile Patriot air defense system with $P_{av} = 10$ kilowatt average power, antenna area of $A_{eff} = 4.5\ m^2$, a noise factor of $F_n = 3$ and a total loss factor of $F_L = 5$. In an anti-tactical ballistic missile defense mode, the solid angle to be searched could be $\Omega = 0.94$ steradian (90° azimuth and 20° to 70° elevation ranges). Let the correction factor be $Q_i = 0.9$; for a target fluctuating only from scan to scan (Swerling case 1), and a cumulative de-

tection probability of 90%, the optimum ratios are $\delta = \Delta / r_1 = 0.042$ and $\rho = R_{DetS} / r_1 = 0.155$. A ballistic missile with 1000 km range would approach with an approximate velocity of $v = 3$ km/s. The cross section of a non-stealthy reentry vehicle could be $\sigma = 0.01$ m^2 (like that of an intercontinental ballistic missile). With these values, the distance r_1 from (4-11) becomes 540 km. Thus the search detection range is $R_{DetS} = 83$ km; for a search-optimized system, the incoming missile is detected at this distance with 90% probability – the remaining flight time to target being only about 30 seconds. The optimum frame time is $T_f = 7.5$ seconds – the distance traveled by the missile during this time is $\Delta = 23$ km. For a radar wavelength of $\lambda = 0.06$ m, the beam solid angle is $\omega = 8 \cdot 10^{-4}$ steradian, therefore there are 1170 beam positions to be taken in one frame time; the dwell time per position is $T_d = 6.4$ milliseconds. With a pulse repetition frequency of $f_p = 1$ kHz (unambigous range 150 km), about 6 pulses could be integrated per target per dwell time. During the time between detection and possible impact, the defense has to: measure the trajectory, compute its further course, compute the interceptor trajectory, take the launch decision, launch the interceptor, and let it fly out to a sufficiently distant intercept point. If the time in question is only 30 seconds, the ability to do this with Patriot-type interceptors is doubtful (see 5.1.5.1).

Defense against an aircraft stands in marked contrast to defense against a ballistic missile. All radar and detection parameters being the same, the cross section could be a hundred times higher, $\sigma = 1$ m^2. The approach velocity could be ten times less, for a slightly subsonic velocity of $v = 0.3$ km/s. The search solid angle could be roughly half its former value ($\Omega = 0.54$ sr for 90° azimuth and 0 to 20° elevation range). Taken together, these give a factor of 1,750 in the cube root of (4-11), and r_1 increases by a factor 12 to $r_1 = 6{,}500$ km. For an aircraft, the theoretical optimum detection range is $R_{DetS} = 1{,}000$ km, the frame time would be $T_f = 15$ minutes, the distance flown during that time $\Delta = 270$ km. Of course, these large theoretical values are unrealistic, if only because the curvature of the earth excludes detection of aircraft at such distances. For realistic air defense radars, frame times are much shorter – optimization with respect to cumulative detection probability is not necessary since the echoes from distances where aircraft have to be detected (i.e., less than 200 km) are strong enough in any case.

To complete the picture, a corresponding value of the search detection range shall be derived for a large, fixed phased-array radar, as is used for early warning of ICBM attacks. The U.S. Cobra Dane radar on Shemya Island of the Aleutians has an average power of $P_{av} = 920$ kW and an antenna area of 340 m^2.[15] For search a solid angle of $\Omega = 0.11$ sr (20° elevation and 20° azimuth ranges) may be appropriate. If the cross section of a reentry vehicle is again taken to be $\sigma = 0.01$ m^2, then, all other parameters being the same, the optimum search detection range would be 2,400 km, with a frame time of $T_f = 94$ s.

4.1.1.4 Detection Using Large Phased-Array Radars

The example of the last section shows that, in principle, large phased-array radars can provide more than sufficient detection range against tactical ballistic missiles – this holds because at fixed sites the antenna area and the power can be much higher than with mobile systems. In Western Europe, one could conceive of one to three such installations in the western part of the Federal Republic of Germany. Because these systems are very expensive, their number will be limited. Because these high-value targets would be within reach of several classes of hostile weapons, it is improbable that they would survive the first attacks. An alternative would be to use the new large phased-array radar being built at Fylingdales in

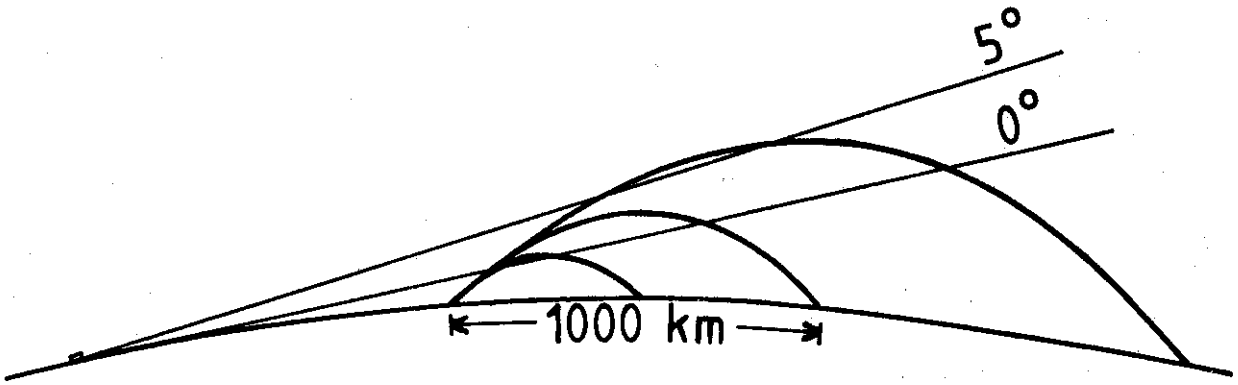

Fig. 4-4 A radar in Scotland (at 1,000 km distance) cannot detect ballistic missiles targeted at West Germany with ranges of up to 1,000 km. Radar performance decreases at some point between 5° elevation and the horizon.

Scotland. This is some 1,000 km from the East-West-German border. As Fig. 4-4 demonstrates, tactical ballistic missiles in Central Europe with ranges up to 1,000 km remain below its horizon; therefore, it could not be used for the most important ranges.

4.1.1.5 Airborne Radars for Detection of Tactical Ballistic Missiles

In principle, airborne radars have a much farther horizon than ground-based ones. Because tactical ballistic missiles of most ranges have maximum altitudes of more than 100 km, this would not present a tremendous advantage, however. More important is the fact that the detection ranges are of the same order of magnitude. This stems largely from the limited amount of electrical power available on board an aircraft. The U.S. Airborne Warning and Control System (AWACS) E-3A aircraft has a generator capability of 600 kVA.[16] Taking into account other consumers of electrical power, the radar transmitter could take on the order of 100 kW, which corresponds to several times 10 kW average radar power. In addition, a ballistic missile search radar requires a beam which is confined in two dimensions. This calls for an antenna of roughly circular (or e.g. quadratic) form, which is very difficult to mount on an aircraft due to its size. (For aircraft detection, the beam need only be strongly confined in the azimuth direction. Thus the AWACS antenna is several times wider than high, and can be built into an oblate circular structure above the fuselage.) A third problem is that such antennae of airborne radars are scanned mechanically at a slow rate (the AWACS antenna at one revolution per 10 seconds)[17], and rapid beam steering to random directions is impossible. Mounting phased-array antenna elements on the fuselage, i.e., a non-plane surface, has several drawbacks and has up to now only been discussed for detecting large, slow ground vehicles.[18] Thus, airborne radar systems do not offer any advantage over mobile ground-based ones.

4.1.1.6 Over-The-Horizon Radars for Detection of Tactical Ballistic Missiles

If a radar system works with relatively long wavelengths (10 – 100 m), it can utilize ionospheric reflection to measure reflexes from objects below its horizon, from a minimum range of about 1,000 km, up to distances of several 1,000 km.[19] Such systems are installed in the USA for the early warning of launches of submarine-launched ballistic missiles.[20] Because of the long wavelengths, antenna fields several hundred meters wide are required. In addition, the angular resolution is poor because of the diffuse reflection process, and frequencies have to be varied according to the momentary ionospheric conditions. Such a system would be a large fixed installation, vulnerable to several classes of conventional weapons. Thus, over-the-horizon radar is unlikely to be used for detection of tactical ballistic missiles.

4.1.2 Short-Wave Infrared Detection of Booster Flames

The hot exhaust gases of rocket motors emit intense thermal radiation, centered in the short-wave infrared region (1 to 5 μm wavelength). This radiation is so intense that it can be detected against the normal background of the earth in most cases; the early warning satellites deployed at geostationary altitudes today are vivid examples of this ability. Some typical properties of the boost phase of different missile types are listed in Tab. 4-3 at the end of 4.1.2.1.

Radiation quantities to be used in the following are:
- radiant flux (i.e., power) Φ, unit: watt;
- radiant exitance M, the quotient of emitted power and area of a source, unit: W/m^2;
- radiance L, the quotient of radiant exitance and solid angle, unit: $W/(m^2\,sr)$;
- irradiance E, the quotient of the incident power and area, unit: W/m^2.

The derivatives of these quantities with respect to wavelength are referred to as "spectral" and are denoted by a subscript "λ" (e.g., the spectral radiance by L_λ, unit $W/(m^3\,sr)$). Radiation quantities are converted into each other by appropriately integrating or differentiating with respect to wavelength, area, and/or solid angle.

The spectral radiance at the wavelength λ of a blackbody at the absolute temperature T is given by

$$L_{\lambda Bb}(\lambda, T) = \frac{2hc^2}{\lambda^5} \frac{1}{e^{hc/(k\lambda T)} - 1}, \qquad (4\text{-}14)$$

where $h = 6.626 \cdot 10^{-34}$ Js, $k = 1.381 \cdot 10^{-23}$ J/K, and $c = 3.00 \cdot 10^8$ m/s. Its total radiant exitance is

$$M_{Bb} = \int_{2\pi} \int_0^\infty L_{\lambda Bb}\, d\lambda\, d\Omega = \sigma T^4 \qquad (4\text{-}15)$$

where $\sigma = 5.67 \cdot 10^{-8}\ W/(m^2 K^4)$.

4.1.2.1 Radiant Emission of Booster Flames

In the combustion chamber of a chemical rocket, a chemical reaction produces hot gases at temperatures of 3,000 to 4,000 Kelvin. These gases develop high pressure and flow through the nozzle; in the nozzle they are expanded and accelerated, whereby thermal energy is partly converted to kinetic energy (i.e. irregular motion is partly converted to regular motion). The thrust force is at maximum if the exit pressure equals the external pressure. Therefore, expansion is limited, and typical conversion efficiencies are about 0.6. Depending on nozzle design and the molecular properties, the exit temperature will lie between 1,000 and 2,000 K. If for an actual missile we take the internal efficiency, i.e., the ratio of kinetic energy of the exhaust gases with respect to the missile to the total thermal energy produced, to be 0.5, then the thermal power of the exhaust gases P_{Therm} equals their mechanical power P_{Thrust}, and is one half of the total thermal power released in the combustion chamber $P_{ThermChamber}$:

$$P_{Thrust} \cong P_{Therm} \cong 0.5\, P_{ThermChamber} \tag{4-16}$$

The remaining thermal power is manifest in the increased temperature of the exhaust gases; after leaving the nozzle, the gases lose thermal energy by radiation and by collisions with the surrounding atmosphere. The visible flame of a rocket is the part of the exhaust gases where the temperature is sufficient for radiation in the visible part of the spectrum. At the nozzle, the gases might have temperatures of 1,800 K; at the margin of the visible flame, the temperature might have fallen to about 1,000 K. A good mean value would be 1,500 K. The size and form of the exhaust plume depend on a number of factors; in the lower atmosphere, its diameter could be 4 times the nozzle diameter and its lengths 20 times the nozzle diameter. In the vacuum of space, expansion of the plume can go much further: it can assume an almost spherical form of some 100 nozzle diameters in size, sometimes even encompassing the missile itself. Fig. 4-5 gives examples of the form of exhaust plumes at 30 km altitude and in free space. Predicting the exact radiative properties of a missile exhaust plume is exceedingly difficult. The different distributions of chemical species, temperature variations, interactions with the atmosphere, self-absorption in the plume and other factors have to be taken into account.[21] For a simple model calculation, however, knowledge of some basic experimental results suffices. The most important fact is that most of the exhaust is in the form of simple molecules like H_2O, CO, or CO_2, which can only emit in distinct wavelength bands. Because in any of these bands the spectral radiance can at most be equal to that of a blackbody at the same temperature, this means that the total amount of radiated power – integrated over the whole spectrum – is significantly less than for a blackbody. In some rocket motors, a significant portion of the exhaust is particulate matter (carbon, and for solid fuels, aluminum oxide particles), which emit like a gray body with a higher temperature (about 1,800 K) and a low emissivity (about 0.03). Fig. 4-6 gives experimental spectral radiances of different model rocket motors, together with the theoretical radiance of a blackbody of 1,500 K. The H_2O and CO emission bands at 2.8 μm and the CO_2 emission bands at 4.3 μm are evident. The continuum in between is partly due to particulate matter.

By doing a rough spectral integration of Fig. 4-6 c) (and an integration over the half solid angle of 2 π steradian, including a factor of 0.5), one can derive that for a solid-fuel rocket, the total radiated power per area, i.e., the radiant exitance, in the infrared between 2.3 and 4.8 μm is only about 4% of that of a blackbody.[22] In each of the two bands, approximately 2% of the total radiant exitance of an equivalent blackbody can be found. With a temperature of

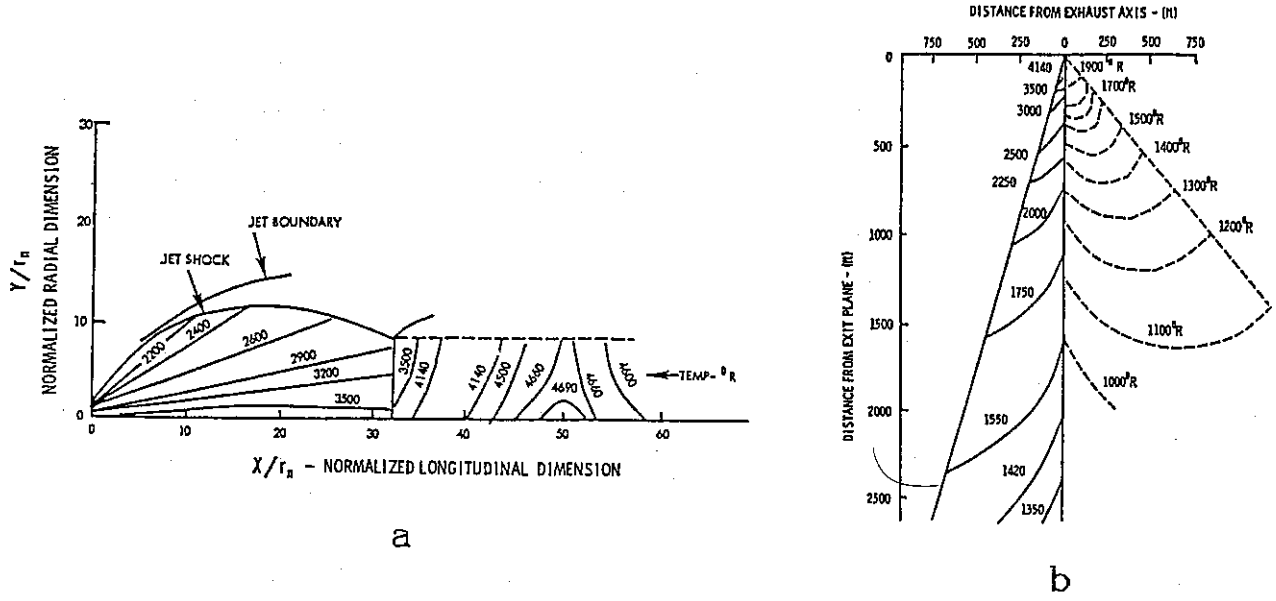

Fig. 4-5 Forms of the exhaust flame of solid-propellant missiles by isotherms for particles.[23]
a) At 30 km altitude, exhaust temperature 6,100° R = 3,390 K, 0.79 μm particles, r_n: nozzle radius.
b) In vacuum, solid lines: 3.94 μm particles, dashed lines: 0.79 μm particles.
1.8 degree Rankine = 1.0 Kelvin, 1 ft = 0.305 meter.

T = 1,500 K, the total radiant exitance after (4-15) is $M_{Bb} = 290\ kW/m^2$. If the spectral peak of Fig. 4-6 around 4.3 μm is 0.3 μm wide, its total radiant exitance becomes $M_{4.3\ \mu m} = 4.6\ kW/m^2$. Using a spectral width of 0.7 μm, the radiant exitance around 2.8 μm is $M_{2.8\ \mu m} = 5.4\ kW/m^2$.

Now the total radiated power Φ can be calculated, if the emitting area A (i.e., the plume surface) is estimated:

$$\Phi = M\,A. \tag{4-17}$$

With a cylindrical flame of 4 meter diameter and 50 meter length (i.e., a surface of A = 600 m^2)[24], the first stage of a solid-fuel ICBM emits about 8 Megawatt power in the infrared, about half of this value in the 4.3 μm and 2.8 μm band respectively. This value is significantly less than the result of an estimation using a blackbody model;[25] it is, on the other hand, significantly more than the figure of "hundreds of kilowatts" which is sometimes quoted.[26] It is interesting to compare this power with the kinetic power of the exhaust gases (which, as remarked above, is approximately equal to their thermal power). The kinetic power is given by the thrust force F_T and the exhaust velocity v_e:

$$P_{kin} = F_T\,v_e = m_0\,(a_0 + g \sin \alpha)\,v_e. \tag{4-18}$$

m_0 is the launch mass, a_0 is the initial acceleration, α is the launch angle of the missile, and g is the gravity acceleration. For the U.S. Minuteman III ICBM, the initial acceleration is about 1 g, the launch angle is 90°; the launch mass is 35 Mg.[27] For vertical launch, the thrust is 690 kilonewton; if the exhaust velocity of the solid fuel is taken to be v_e = 2.5 km/s, then the kinetic power is 1.7 gigawatt. This means that only about 0.5% of the kinetic (or thermal) power is radiated in the short-wave infrared. The other portion of the thermal energy re-

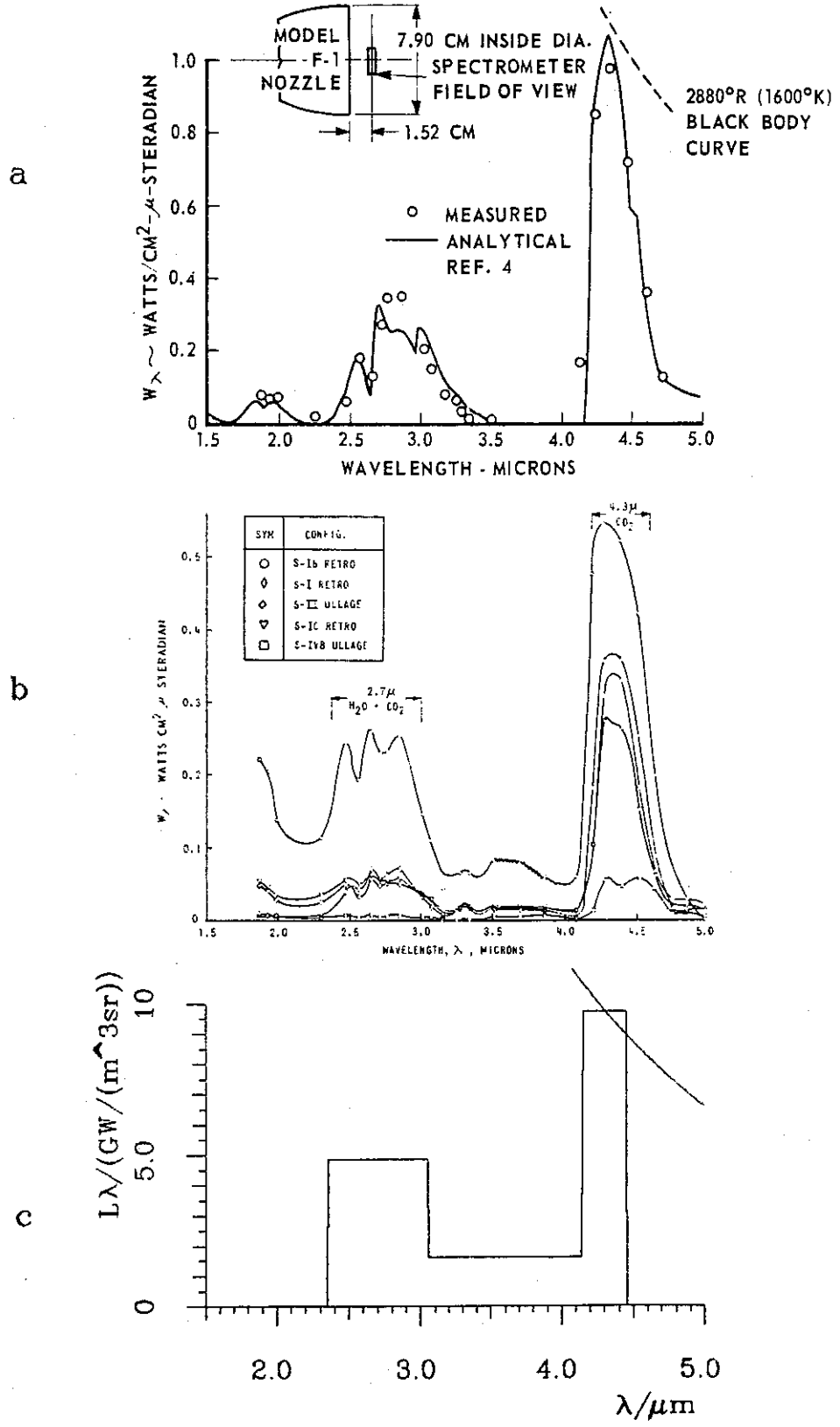

Fig. 4-6 Spectral radiance L_λ of liquid (a) and solid (b) rocket motors as measured on model engines.[28] Note that for solid fuel, the absolute values are lower by a factor 2 – 3. The simplified model spectrum for calculation purposes is shown in (c), together with the spectral radiance of a blackbody at the plausible mean temperature of T = 1,500 K temperature (for solid fuel, it is multiplied by 0.5). 1 W/(cm^2 μm sr) = 10^{10} W/(m^3 sr).

leased is dissipated by non-radiative processes or by weaker long-wave infrared radiation after the gases have cooled somewhat. The figure of 1% of the kinetic power can be used as a rule of thumb for estimating the infrared radiant power for other kinds of missiles as well. Table 4-3 gives estimates for burn times, sizes, and kinetic powers of missiles of different range categories. The infrared radiant power values of the last column have been conservatively taken to be 1% of the kinetic powers.

Tab. 4-3 Boost phase properties of different missile categories – typical estimated values (variations are possible with different missile types and payloads). Burnout altitude is for the last stage, whereas the other numbers hold for the first stage. In general, each following stage is smaller by a factor of between 1.5 and 5, whereas the burn times are roughly equal. By increasing the thrust (and thus the power), burn times and burnout altitudes can be reduced. The last column gives the total infrared radiant power which is divided between the 2.7 and 4.3 μm bands and a small continuum portion. Note that the motors of short-range ballistic missiles often have two burn phases: a short intense boost phase for the initial acceleration, and a longer sustain phase with reduced thrust to overcome the air drag.

	Range km	No. Stages	Last Stage Burnout Altit. km	First Stage Burn Time min	First Stage Nozzle Diam. m	First Stage Kinetic Power GW	First Stage IR Radiant Power MW
Intercontinental ballistic missile	10,000	2–4	150	1.5	1.5	2	20
Intermediate range ballistic missile	2,000	2	100	1	0.5	0.5	5
Tactical ballistic missile	1,000	2	50	1	0.5	0.3	3
Short range ballistic missile	100	1	20	0.3	0.3	0.2	2

4.1.2.2 Detection of Infrared Emission from Booster Flames

The booster flame emission can be sensed by an infrared detector on board a satellite, if the optical system collects sufficient light power from the flame so that this signal is above the noise. The power on the detector Φ_D is (under the assumption of isotropy)

$$\Phi_D = \Phi_{Source} \frac{A_{Optics}}{4 \pi r^2 F_L}, \tag{4-19}$$

where Φ_{Source} is the power emitted within the spectral interval of the detector, r is the distance, and F_L is the loss factor in the optical system of area A_{Optics}. If the optics has a diameter of 1 meter and a loss factor of 2, for a geostationary satellite (distance about 40 megameter) the infrared power on the detector would be 400 picowatt ($400 \cdot 10^{-12}$ W) for an ICBM, and 40 picowatt for a short-range missile. With a mean photon energy of

$$E_{Ph} = h\,c/\lambda = 5 \cdot 10^{-20} \text{ joule} \tag{4-20}$$

($h = 6.62 \cdot 10^{-34}$ Js, $c = 3 \cdot 10^8$ m/s, $\lambda = 4$ μm) these powers translate into photon currents of $8 \cdot 10^9$/s or $8 \cdot 10^8$/s, respectively. The background against which this signal has to be detected is

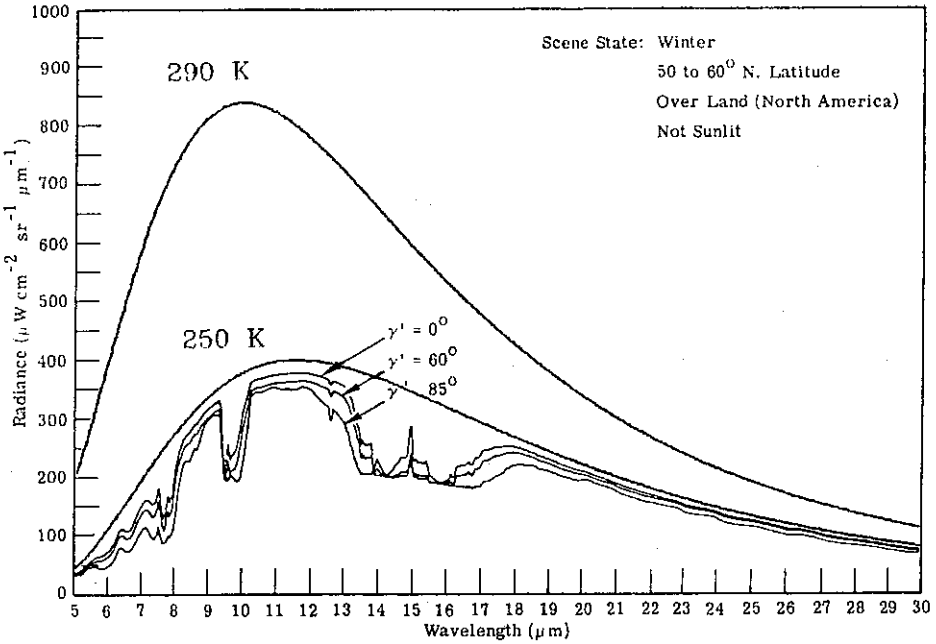

Fig. 4-7 Calculated infrared emission spectrum from the earth and atmosphere as seen from space (winter, 50-60° latitude, over land, not sunlit, $\gamma' = 0$ for looking vertically downward).[29] For comparison, the radiant spectral densities of blackbodies at 250 and 290 K temperature have been added. 1 $\mu Wcm^{-2} sr^{-1}\mu m^{-1} = 10^4 W/(m^3 sr)$.

the infrared radiation of the earth including the atmosphere (background radiation from the optics can be kept lower by appropriate cooling) (Fig. 4-7). If, for a moment, we take the earth-atmosphere system to be a blackbody at T = 290 K temperature, then the integrated radiant exitance in the wavelength band from 2.5 to 4.6 μm is calculated to be $M_{Bg} = 2$ W/m^2; if the optics images an area A_{FOV} of the earth (vertical projection) onto the detector, the background power on the detector becomes

$$\Phi_{Bg} = M_{Bg} A_{FOV} \frac{A_{Optics}}{\pi r^2 F_L}, \tag{4-21}$$

which is $\Phi_{Bg} = 16$ nanowatt for a field of view of $A_{FOV} = 10^8$ m^2 (10 km squared). This is more than 60 times the signal power from an ICBM. In order to be detectable, however, the signal need not be above this mean power, but only above the fluctuations of this background power, its root-mean-square variation. With a mean photon energy E_{Ph}, this noise power is given by [30]

$$\Phi_{BgN} = \left(\frac{2\,\Phi_{Bg} E_{Ph} B}{\eta}\right)^{1/2}, \tag{4-22}$$

where B is the bandwidth of the detection system and η is the quantum efficiency of the detector. If these values are taken to be B = 1 Hertz and $\eta = 0.5$, then with $E_{Ph} = 5 \cdot 10^{-20}$ J the noise power becomes $\Phi_{BgB} = 6 \cdot 10^{-14}$ watt for the above case of $A_{FOV} = 10^8$ m^2. This is several orders below the signal power for an ICBM and still well below the signal of a short-range missile.

In reality, however, the earth and the atmosphere can show strong deviations from blackbody radiation. In the present context, conditions where the radiance is far above the blackbody value will have the most negative influence on the detection of missile plumes. Large

deviations can ensue if sunlight is scattered on snow or at cloud tops, or if it is reflected at a rough water surface where the reflection law is fulfilled for parts of the waves. For low incidence angles, the spectral luminance factor of a water surface in the "light trail" can even approach unity.[31] If, as an extreme case, I assume that looking into the sun glint is equivalent to looking directly into the sun (approximated by a blackbody of 5,900 K temperature), the 1 m diameter optics collects about 1.17 kW total power and focusses this on an image in the focal plane which, with 3 m focal length, has 2.7 cm diameter; a detector of 1 mm^2 would be hit by about 1 watt – which after several seconds might even destroy it. If a spectral filter transmits only infrared wavelengths between 2.5 and 4.6 μm, the power on the detector is reduced to 0.026 W; with a further reduced spectral window from 4.3 to 4.6 μm, the power on the detector would be 1.4 milliwatt. This is more than a million times the signal power. In order to prevent overloading or even damaging the detector and preamplifier, a shutter or iris would have to be closed. In any case, such strong background signals would preclude detection.

The effect of specular reflection of sunlight on water can be reduced by a number of factors: First, clouds can prevent the sunlight from penetrating as a direct beam (this can create the problem of sun reflection from cloud tops, see below). Second, atmospheric absorption decreases the beam power in certain wavelength regions; if the detector is equipped with a filter which transmits only those wavelengths that are strongly absorbed by the atmosphere, the spurious signals can be suppressed. Third, a system designed to detect launches of short- and intermediate-range missiles has to look upon land, not upon water areas.

Next, I want to estimate the amount of infrared power reflected by snow and clouds (for snow, atmospheric absorption can effect drastic reductions, but the signals of high clouds can propagate essentially undiminished to space). If the albedo (i.e., the ratio of outgoing to incoming radiative power) of such a white diffuse reflector is 1 (this ideal value is not far from reality in several cases)[32], then its spectrally integrated radiant exitance is $M_{tot} = 1.4$ kW/m^2, equal to the integrated sun irradiance at the margin of the atmosphere. Within a spectral window from 2.5 to 4.6 μm, the reflected radiant exitance is $M_{2.5-4.6\ \mu m} = 40$ W/m^2; within a 0.3 μm wide window around 4.3 μm, the radiant exitance is $M_{4.2-4.5\ \mu m} = 2.2$ W/m^2. Using (4-21) with a field of view $A_{FOV} = 10^8$ m^2, a detector with a 1 m diameter optics and a loss factor $F_L = 2$ at $r = 40$ Mm distance, receives 11 mW integrated power. If a filter reduces the wavelengths detected to the interval from 2.5 to 4.6 μm, this power decreases to 320 nW, about 800 times the power received from an ICBM first stage flame. If the spectral interval is confined to a 0.3 μm wide band around 4.3 μm, the reflected signal is further reduced to 17 nW, a factor 100 above an ICBM signal. Since this reflection can change with time in an unpredictable manner, boost flame detection would require that the signal were above these background variations – which, as shown, is not the case if the reflected sun power propagates unhindered to space. A way out of this problem is, however, possible by atmospheric absorption, at least for reflectors at low altitudes.

Predicting the atmospheric extinction is an extremely complicated process. Because the molecular absorption is a rapidly changing function of wavelength (in the low atmosphere, linewidths are in the order of 0.001 μm, and can be much lower at higher altitudes), for an exact spectral integration the source spectrum has to be known with the same high degree of resolution. Water content varying with altitude, season, and climate, further complicates the picture. The other contributions to extinction, namely molecular scattering and aerosol absorption and scattering, show a much smoother dependence on wavelength.[33] Fig. 4-8 shows broad-band absorption spectra of atmospheric gases and of the atmosphere. Fig. 4-9 gives

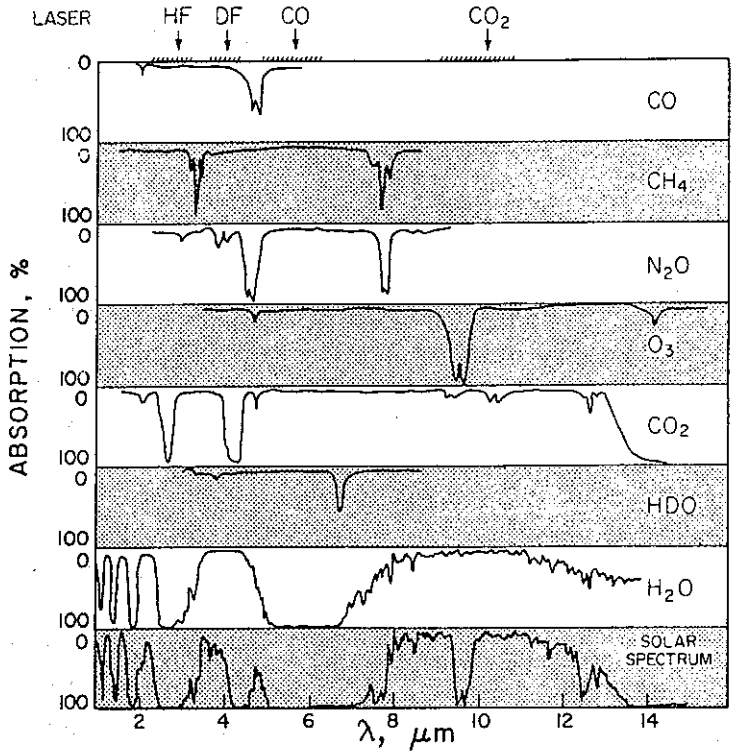

Fig. 4-8 Absorption spectra of different atmospheric gases and of the total atmosphere.[34]

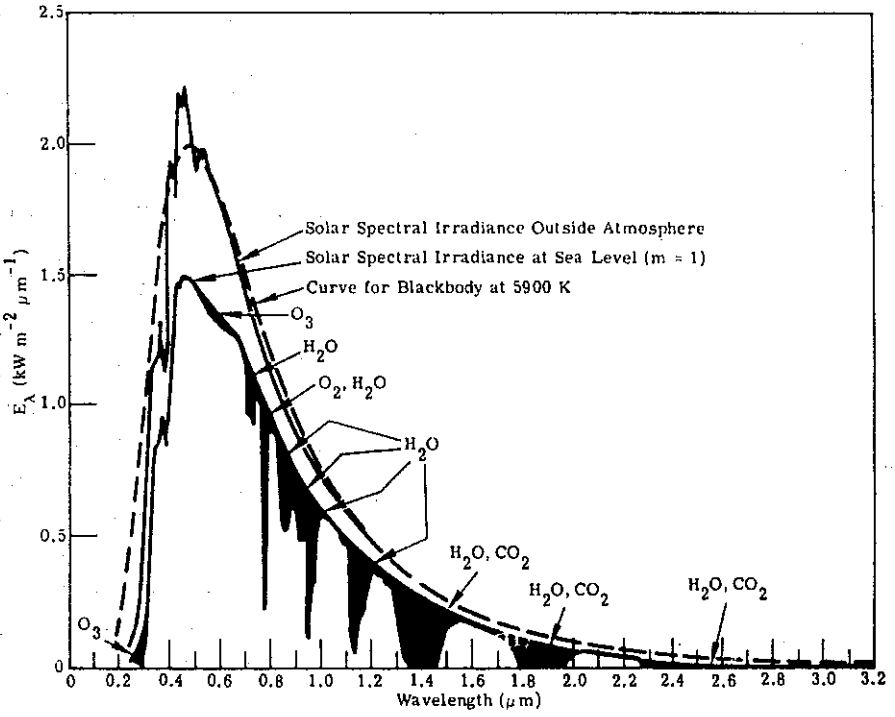

Fig. 4-9 Influence of the atmospheric absorption on sunlight is shown in these solar irradiance spectra measured outside of the atmosphere and on the ground.[35] For comparison, a blackbody spectrum at 5,900 K has been drawn too. Absorption due to different atmospheric constituents is indicated. 1 kW m^{-2} μm^{-1} = 10^9 W/m^3.

the solar spectrum as received on the ground. In order to gain a rough idea on the absorption of rocket exhaust radiation, one can treat this emission as quasi-continuous in the 2.7 and 4.3 μm bands. Using the simplified method of Ref. 36, one can deduce that for transmission through the whole atmosphere (i.e., a vertical path one-way), in the 2.5 to 2.8 μm band as well as in the 4.2 to 4.5 μm band the transmissivity is below 0.01, in some regions less than 0.001. For transmission down to 5 km, in the band around 2.7 μm, the transmissivity increases up to about 0.1, whereas around 4.3 μm it is still below 0.01. For 10 km altitude, in the 2.7 μm band the transmissivity is well above 0.1, and the portion of the band around 4.3 μm, where the transmissivity is below 0.01, shrinks considerably. For altitudes of 30 km or higher, the infrared power is attenuated by a factor of 2 at most. A slant path from medium latitudes to a geostationary position is inclined from the vertical by about 30°, thus the effective pathlength increases only by a factor of about 1.2.

These figures mean that by using appropriate filters, the signals from some background sources can be reduced drastically. If these filters block all radiation except in the regions where the atmosphere is opaque, the infrared reflections from water or snow at sea level can be reduced by a factor of $1 / 0.01^2 = 10^4$ at least. The power calculated above for the 4.3 μm band thus decreases to $2 \cdot 10^{-12}$ W, which is 200 times less than an ICBM signal and 20 times less than the signal from a tactical ballistic missile. (Of course, these flame signals obey the same attenuation, and the missiles will only become visible when they are at sufficient altitude. For all but the shortest range missiles, this should not present a significant detection problem, since burnout is well above 30 km.) This picture changes if dense high clouds exist – cirriform ice clouds regularly exist in 6 to 12 km altitudes but are only seldom dense; sometimes the top of the dense cumulonimbus clouds reaches up to 12 km. For such situations, the scattered sun signals in the infrared bands in question will remain more or less unattenuated by atmospheric extinction. These effects have obviously limited the usefulness of infrared early warning sensors on geostationary satellites from time to time; television cameras sensitive in the visible region have been employed in parallel to assist in rejecting spurious infrared signals.[37]

Table 4-4 summarizes the numerical estimates of the detector power for the different sources. More specific statements on the strengths of the signals from ballistic missiles and on the background noise would require exact knowledge of the filter and detector bands, as well as of the emission spectra of the booster flames. Much of this is classified. For the purposes of the present study, however, one can conclude that detection of the exhaust flames of tactical ballistic missiles should be possible in most cases, but that the tenfold reduced signal poses more stringent requirements for background reduction than are required for early warning of ICBM launches. It may be necessary to increase the resolution to a field of view of less than 10 km squared; for a staring mosaic detector covering Central Europe (roughly 1,000 km by 1,000 km), a 1 km^2 field of view would mean a cell number of 10^6 – this is two orders of magnitude above the present state of the art for two-dimensional cooled infrared detector arrays.[38] For missiles with less than 500 km range, it may be possible to shorten the boost phase such that it ends after a couple of seconds at less than 30 km altitude, and to overcome the air drag by a strongly reduced sustainer burn. Thus, boost flame detection from space could possibly be prevented.

In principle, staring mosaics open several additional possibilities for background suppression by using context information, e.g., by forming tracks from consecutively illuminated cells. This, however, would require the solution of several considerable problems concerning computers and algorithms.[39]

Tab. 4-4 Comparison of infrared powers from different sources, impinging on a detector of 1 mm^2 area with an optics of 1 m diameter and loss factor 2 at 40 megameter distance, in different bands of the infrared spectrum (see text).

Signal source and band	Power on detector in watt
Fluctuations of the earth-atmosphere background, 2.5–4.6 μm	$6 \cdot 10^{-14}$
Short-range ballistic missile, 2.5–4.6 μm	$4 \cdot 10^{-11}$
ICBM first stage, 2.5–4.6 μm	$4 \cdot 10^{-10}$
Reflection from high clouds (10^8 m^2 field of view), 0.3 μm around 4.3 μm	$2 \cdot 10^{-9}$
2.5–4.6 μm	$3 \cdot 10^{-7}$
Direct sunlight, 0.3 μm around 4.3 μm	$1.4 \cdot 10^{-3}$
2.5–4.6 μm	$2.6 \cdot 10^{-2}$

4.1.2.3 Some Geometrical Considerations

The field of view A_{FOV} of one detector element is given by its area A_D, the focal length f of the optics and the distance r from the earth:

$$A_{FOV} = A_D \frac{r^2}{f^2}. \tag{4-23}$$

Using a typical value of f = 6 m focal length and a detector side length of 0.1 mm (which is far above the diffraction limit for optics of 1 m size), for a geostationary observation satellite (r = 40 Mm), the field of view could become as low as $A_{FOV} = 4.4 \cdot 10^5$ m^2 (0.4 km^2, a square of 670 m side length). Thus, quite small fields of view, and significant reductions of the spurious sun reflections from clouds or snow, are possible in principle. On the other hand, the number of scene elements to be looked at increases, as the size of the elements decreases. The area in Eastern Europe from where missiles of up to 1,000 km range could be launched, is approximately 1,000 km deep and 1,000 km long. Looking at this area of roughly 10^6 km^2 with a linear array of 1,000 elements which is scanned periodically, would be similar to the traditional early warning technology: Here a linear array of 2,000 elements is scanned, and the field of view of every element is about 5 km^2.[40] In order to gain the full advantages in noise reduction and context-dependent information processing, a staring array would have to have about 10^6 detector elements, which for cooled infrared detectors, as stated above, is far from being available.

A geostationary early warning satellite which can detect the exhaust plumes of missiles when they penetrate the cloud cover, or rise above about 30 km, with 1 km resolution, could provide knowledge of the launch areas with a few km accuracy. Measuring the trajectory during the boost phase is nearly impossible, because only very few detector elements may be involved. Therefore, although a rough guess on the direction may be done, no estimate on the missile velocity and thus on its range can be made. In principle, two such early warning satellites, deployed at different longitudes, could provide stereoscopic measurements of the

consecutive locations of the missile with a few km accuracy, but this would require a very complicated and costly system and will therefore probably be avoided.[41] Knowing the launch areas of missiles could, nevertheless, provide valuable clues for the search radars of ground-based missile defenses, because the missile trajectories are bound to lie in the plane defined by the launch and impact points, and the center of the earth. Therefore, if the launch position(s) could be relayed quickly to the defenses on the ground, their radars could confine the azimuth search positions to those angles which point to the launch areas. (Of course, if massive launch activity from many different places takes place, no significant savings in azimuth search will be possible.)

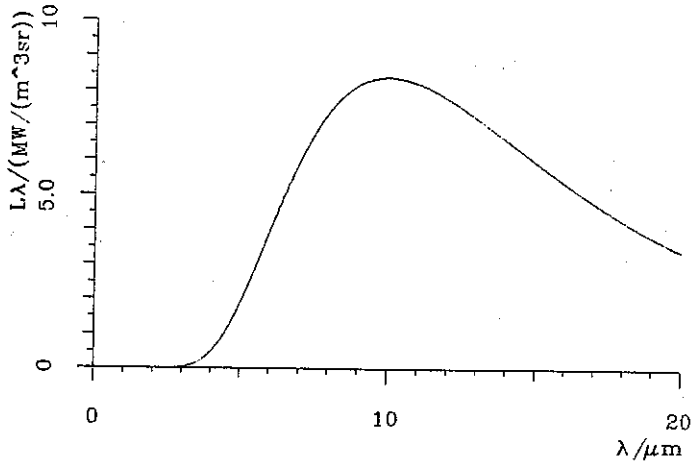

Fig. 4-10 Spectral radiance of a blackbody at 290 K temperature.

4.1.3 Search by Long-Wave Infrared Detection After the Boost Phase

Another possible search method is to look for the missiles or reentry vehicles as they coast through space. In this case, the temperature of the objects is much lower than the hot gases of the booster flames; therefore the emission takes place at longer infrared wavelengths, and with reduced power. Whereas a short-range missile may still have an elevated temperature from air friction, reentry vehicles which have been under a shroud during the boost phase, will remain at approximately room temperature. (Incidentally, this is also the equilibrium temperature for a sunlit object in near-earth space.) Fig. 4-10 gives the spectral radiance of a blackbody at T = 290 K temperature, which represents a good approximation to the actual properties of reentry vehicles. The spectral maximum is at 10 μm; infrared detectors have to be chosen which are sensitive in the 8 to 12 μm region (e.g., HgCdTe or Ge:Au detectors). The total radiative power emitted by a gray object of 1.7 m^2 area (e.g., a cone of 1.5 m length and 0.6 m base diameter) and emissivity 0.9, after (4-15) and (4-17), amounts to 620 W; in the region between 8 and 12 μm, the radiated power is 160 W, which is a factor 10^4 below the power (in the 2.5 to 4.6 μm band) of a booster flame of a short-range missile. (In the 10.6 to 12.6 μm band to be considered later, the radiated power is 80 W.) Because the temperature of the object is comparable to that of the earth and its atmosphere, it is not possible to detect missile bodies or reentry vehicles from above, against the background of the earth. Therefore, it is envisaged that long-wave detectors be flown on satellites in low orbits (or maybe popped up on rockets) which look horizontally, or on board high-altitude aircraft where they look upward. In both cases the background would be cool dark space.

4.1.3.1 Signal and Noise Powers

If isotropic radiation is assumed, the infrared power on the detector can be calculated from (4-19) (for viewing a cone head-on, the effective emitted power may be somewhat lower). If the collecting optics has 1 m diameter and a loss factor 2, the signal power impinging on the detector from 100 km distance is 500 pW ($500 \cdot 10^{-12}$ W). From 500 km distance, this value drops to 20 pW. In order to determine whether such low powers can be detected, one has to analyze several possible sources of noise. Thermal radiation within the detector material can be kept at negligible levels through cooling. The same holds for the thermal resistance noise in the detector and the first amplifier stage. Background radiation can come from the scene looked at (in the present case, this could be radiation from stars, from aurorae or high clouds), and especially from the optics: the detector senses thermal radiation emitted by the mirrors, tubes and baffles as well as by windows in the optical system. It can be reduced by providing a cooled aperture in front of the detector, which reduces the solid angle from which thermal radiation from the surroundings can hit the detector, and by adding a cooled filter, which transmits only in a certain wavelength interval.

For a spaceborne long-wave infrared system, the optical system could be built without a window and be cooled to temperatures of 5 Kelvin; thus even faint stars would become detectable.[42] For an airborne system, in order to be able to cool the optical system without condensation occurring, a window must isolate the system from the surrounding air. Residual thermal radiation emitted by the window which is not totally transparent can, in this case, be the dominant source of background noise. The noise power Φ_N of an optical detector is defined as the amount of radiation power which, when impinging onto the detector, would produce an electrical signal equal to the root-mean-square of the electrical noise in the absence of signal radiation. In case of a background-noise limited infrared photon detector, the noise power is proportional to the square root of its area A_D and of the detection bandwidth B; the inverse of the constant of proportionality is called the specific detectivity D*:

$$\Phi_N = \frac{(A_D\, B)^{1/2}}{D^*}. \qquad (4\text{-}24)$$

D* is determined by the cutoff wavelength λ_c of the detector material, by the amount of background radiation sensed, and by the opening angle of the cooled aperture. For most semiconductor materials, the quantum efficiency η is constant with wavelength; in this case, D* increases linearly with wavelength up to a maximum value at the cutoff wavelength. If an ideal bandpass filter transmitting wavelengths from λ_1 to λ_c is sufficiently cooled, its thermal radiation can be neglected. If the (photovoltaic) detector looks on a background at temperature T having an emissivity ε, the maximum specific detectivity is given by[43]

$$D^*(\lambda_c) = \frac{\lambda_c}{2\,h\,c}\left(\frac{\eta}{\pi\,c}\right)^{1/2}\left(\int_{\lambda_1}^{\lambda_c} \frac{\varepsilon}{\lambda^4\,(e^{h\,c/(k\,\lambda\,T)} - 1)}\,d\lambda\right)^{-1/2} F(2\,\Theta). \qquad (4\text{-}25)$$

$h = 6.62 \cdot 10^{-34}$ Js is Planck's constant, $c = 3.00 \cdot 10^{8}$ m/s is the velocity of light, and $k = 1.38 \cdot 10^{-23}$ J/K is Boltzmann's constant. The factor $F(2\,\Theta)$ describes the solid angle reduction; in theory,

$$F(2\Theta) = \frac{1}{\sin\Theta}. \tag{4-26}$$

In reality, it approaches about 3 as the full opening angle 2Θ decreases below 30°.[44] As a guide, let us assume a theoretical detector with quantum efficiency $\eta = 0.5$ and cutoff wavelength $\lambda_c = 12\ \mu m$, looking through a cooled filter transmitting from $\lambda_1 = 8\ \mu m$ to $\lambda_c = 12\ \mu m$ with an opening angle of $2\Theta = 30°$. If it looks on a window at $T = 300$ K temperature which has a value of transmittance plus reflectance of 0.99, i.e., an emissivity of $\varepsilon = 0.01$, the maximum specific detectivity becomes

$$D^*(\lambda_c) = 9{\cdot}10^{11}\ \text{cm}\sqrt{\text{Hz}}/\text{W}. \tag{4-27}$$

(The same value results if the background is a mirror at 300 K with emissivity 0.01.) A typical detector element size in a linear array could be $A_D = 0.01\ mm^2$. A typical detection bandwidth for a mechanically scanned linear array could be $B = 100$ Hz (1,000 positions scanned within 10 or 20 seconds). From (4-24), the noise equivalent power is

$$\Phi_N = 10^{-13}\ \text{W}, \tag{4-28}$$

which is significantly lower than the signal power from a distance of 500 km in the 8 to 12 μm band. (With a staring two-dimensional mosaic detector array, bandwidths smaller by a factor of 100, could further reduce this value by a factor of 10.)

Another main source of background noise for an airborne infrared detection system will be the emission from the atmosphere. Of course, the aircraft will have to fly above the dense clouds (but note that high cirrus clouds have produced spurious signals for flight altitudes as high as 13 km)[45]. Airborne infrared measurements at 15° elevation and at altitudes from 8 to 13 km compared well with model calculations.[46] The calculated spectral radiance at 12.2 km (Fig. 4-11) has a peak of $L_\lambda = 1.1{\cdot}10^6\ \text{W}/(\text{m}^3\text{sr})$ at 9.5 μm. The integrated radiance in the 8 to 12 μm band can be estimated to be $L_{8\text{–}12\mu m} = 1.3\ \text{W}/(\text{m}^2\text{sr})$. In order to avoid the prominent emission peak, one could confine the band to wavelengths above 10.6 μm. The integrated radiant density in the 10.6 to 12.6 μm band has been measured directly; its value at 12.2 km altitude is $L_{10.6\text{–}12.6\mu m} = 0.03\ \text{W}/(\text{m}^2\text{sr})$. (Values at 8 km are roughly 10 times higher.) The infrared power Φ_D impinging on a detector of area A_D which looks through an optical system of area A_{Optics}, focal length f, and loss factor F_L at a radiance L is given by

$$\Phi_D = L\frac{A_{optics}\,A_D}{f^2 F_L}. \tag{4-29}$$

With an optical system of 1 m diameter, $f = 3$ m focal length and $F_L = 2$, and a detector of $A_D = 0.01\ mm^2$ area, the powers from sky background in the two bands become

$$\Phi_{D,\,8\text{–}12\mu m} = 6{\cdot}10^{-10}\ \text{W}, \text{ and}$$

$$\Phi_{D,\,10.6\text{–}12.6\mu m} = 1.3{\cdot}10^{-11}\ \text{W}, \tag{4-30}$$

respectively. These signals fluctuate with frequencies from 1 Hz upward during flight, with a relative amount of not more than $7{\cdot}10^{-5}$ to 10^{-3} (which is roughly a factor of 100 above the photon fluctuations one would expect with a constant source), because of small variations in temperature and water vapor content.[47] Taking $5{\cdot}10^{-4}$ as a mean value, the background noise powers become

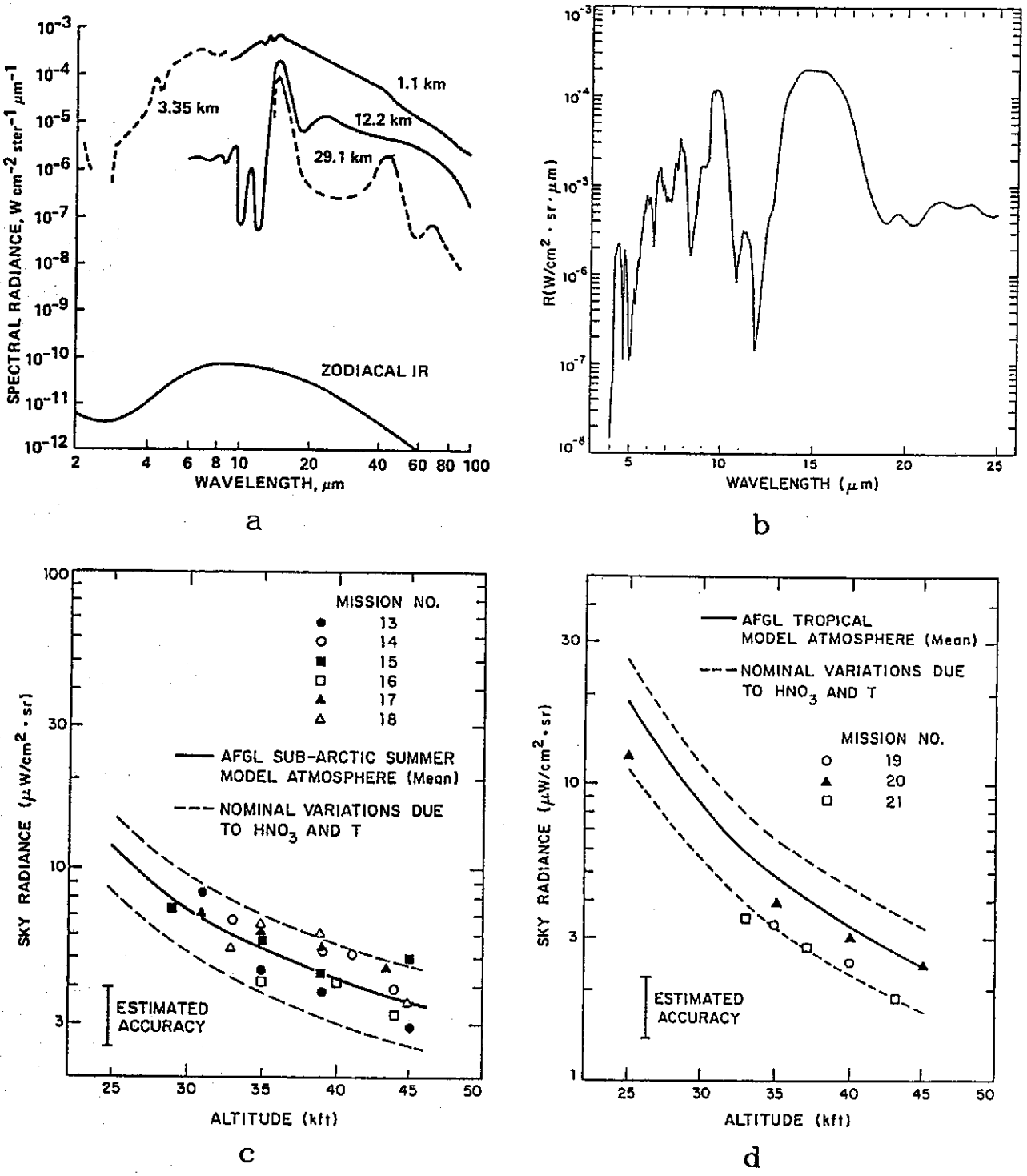

Fig. 4-11 Infrared sky radiance at different altitudes.
a) Spectral radiance as seen by telescope at different altitudes and outside of the atmosphere.[48]
b) Calculated spectral sky radiance at 12 km altitude and 15° elevation.[49]
c) Measured sky radiance in 10.6–12.6 μm band versus altitude, subarctic summer atmosphere, 15° elevation.[50]
d) Measured sky radiance in 10.6–12.6 μm band versus altitude, tropical atmosphere, 15° elevation.[51]
1 W/(cm²srμm) = 10^{10} W/(m³sr); 1 W/(cm²sr) = 10^4 W/(m²sr).

$\Phi_{N,\,8\text{–}12\mu m} = 3 \cdot 10^{-13}$ W, and

$\Phi_{N,\,10.6\text{–}12.6\mu m} = 7 \cdot 10^{-14}$ W. (4-31)

This is of the same order of magnitude as the noise power estimated for the window. In order to fully utilize the detection capabilities of the system, it will thus be necessary to fly at even higher altitudes than 13 km.

In order to estimate the detection range of the long-wave infrared search scheme, the signal power from (4-19) has to be compared to the noise power. If (4-19) is divided by the noise power and solved for the distance, then for given signal-to-noise ratio (S/N) for appropriate detection and false alarm probabilities, the detection range becomes

$$R_{Det} = \left[\frac{\Phi_{Source} A_{Optics}}{4 \pi F_L \Phi_N (S/N)} \right]^{1/2} . \quad (4\text{-}32)$$

If a reentry vehicle emits a power in the 8 to 12 μm band of $\Phi_{Source} = 160$ W, the optics diameter is 1 m, the loss factor is $F_L = 2$, and (S/N) is required to be 10, then the noise power from the window (on a 0.01 mm^2 detector with 100 Hz bandwidth) is $\Phi_N = 10^{-13}$ W, and the detection range R_{Det} becomes

$R_{Det} = 2{,}200$ km, (4-33)

which is a considerable distance. (The U.S. Airborne Optical System has an optics diameter of about 0.5 m;[52] with the same detector size and bandwidth, this would result in about half the values estimated above.)

Now, the detection range shall be calculated if the dominant noise source is the atmosphere seen from an aircraft at 12 km altitude. With (4-31), these ranges become

$R_{Det,\,8\text{–}12\mu m} = 1{,}300$ km, and

$R_{Det,\,10.6\text{–}12.6\mu m} = 1{,}900$ km (4-34)

(where for the 10.6 to 12.6 μm band the appropriately reduced source power has been taken). Because these are rough estimates of the clear air fluctuation only, the flight altitudes of long-wave infrared search aircraft will probably have to be higher than 12 km. Towering cumulonimbus clouds or relatively dense cirrus clouds, can force the aircraft to an altitude in excess of 15 km in any case. For the Airborne Optical System tests, flight altitudes of up to 20 km are envisaged.[53]

A last class of infrared sources deserves analysis: the astronomical objects. If the color temperatures of the objects are identical to that of the sun (which holds for the sunlight reflected by the moon and the planets, and for many stars), their irradiances $E_{\Delta\lambda}$ at the margin of the atmosphere in any spectral region $\Delta\lambda$ can be calculated from the sun irradiance $E_{\Delta\lambda Sun}$, and from the visual magnitude m_v of the object and that of the sun, $m_{vSun} = -26.8$:[54]

$$E_{\Delta\lambda} = 10^{0.4(m_{vSun} - m_v)} E_{\Delta\lambda Sun}. \quad (4\text{-}35)$$

For the spectral region from 8 to 12 μm, the sun irradiance at the earth (modelled as a blackbody of T = 5,900 K temperature, which is a good approximation) becomes

$$E_{Sun,\ 8\text{–}12\mu m} = 1.4\ W/m^2. \quad (4\text{-}36)$$

For a star of the magnitude of the brightest star (Sirius) with $m_v = -1.4$, the irradiance is

$$E_{8\text{–}12\mu m} = 1.5 \cdot 10^{-9}\ W/m^2. \quad (4\text{-}37)$$

(Sirius itself has a higher color temperature and would require calculation with a different spectrum.) For the planet Venus (maximum magnitude $m_v = -4.4$), this value has to be multiplied by 16. Irradiances like this are significantly above that of a reentry vehicle at 500 km distance and will thus be detected easily. Because the objects looked at move with high velocity, it should be possible, after a time, to distinguish them from stars on account of varying location, and irradiance. For the sun which is nine orders of magnitude brighter, the irradiance will be so high that detection of reentry vehicles will be excluded (and a shutter will have to be closed in order to avoid damage to the detector). Table 4-5 compares the detector powers in the 8 to 12 μm band from several sources. (For calculating the detector power for extended objects like the sun or the moon, the power after (4-19) has to be reduced by the ratio of the detector area, to the area of the image produced in the focal plane.)

In conclusion, the principle of long-wave detection of missiles or reentry vehicles from low flying satellites or high flying aircraft can – in the absence of countermeasures – give search ranges of well in excess of 1,000 km. In order to achieve this, aircraft have to fly at altitudes above those used by normal commercial aircraft; this will lead to large wings and light-weight structures which are not capable of rapid maneuvers and may have difficulties with take-off and landing in strong winds (similar to the U-2 and TR-1 aircraft)[55].

Tab. 4-5 Values of the detector power in watt at the margin of the atmosphere in the 8 to 12 μm band, from several sources. Calculation after (4-19) or (4-29), with detector area $A_D = 0.01\ mm^2$, focal length f = 3 m (i.e., viewing solid angle $1.1 \cdot 10^{-9}$ steradian), optics diameter 1 m ($A_{Optics} = 0.79\ m^2$), and a loss factor $F_L = 2$. For extended objects, only the portion of the image hitting the detector has been taken.

Source	Detector power in 8–12 μm band, watt
Noise power from looking through cooled filter onto room temperature window/ mirror of 1% emissivity	10^{-13}
Fluctuations of clear atmospheric background at 12 km altitude	$3 \cdot 10^{-13}$
Reentry vehicle at 500 km distance	$2 \cdot 10^{-11}$
Moon	$2 \cdot 10^{-11}$
Bright star	10^{-10}
Sun	$9 \cdot 10^{-6}$

4.1.3.2 Long-Wave Infrared Detectors on Unmanned Platforms or Rockets

For the purpose of carrying upward-looking long-wave infrared detector systems, remotely or automately piloted vehicles could also be used. This could lower costs and reduce the effort connected with human presence. One has to bear in mind, however, that the optical sys-

tem is large and heavy; its diameter is about 0.5 meter, a motorized gimbal mount is necessary to provide changes of direction and decoupling from carrier movements, and cryogenic cooling of a relatively large focal plane assembly is required. Therefore, such unmanned aircraft would equally be very large, slow to maneuver, and sensitive. Plans for long-wave infrared detector drones included a detector system mass of 7,000 kg (or 10,000–15,000 kg); launch mass was estimated to be 55,000 kg, and the wing span was projected to be 74 meter.[56]

Another possibility is to "pop up" a long-wave infrared detection system on board a rocket as soon as a missile attack is underway or warnings have been received. Because the detection system for search has to be bulky and heavy, this would require a large rocket. The SDI Organization funds research and development of a "long-wave infrared probe" for a ground-based strategic defense architecture based on kinetic energy weapons; it would not seem to be included in the regional (theater) architectures.[57] This is consistent with the fact that due to the short flight times of tactical ballistic missiles, pop-up sensors would have difficulties in arriving at their viewing position in time. In addition, such a large missile with a very expensive detector system would cost many times more than a tactical ballistic missile equipped with a conventional warhead. For these reasons, it seems improbable that large rockets with infrared detectors for search will be utilized in an anti-tactical ballistic missile defense scheme.

4.1.4 Detection Using Laser Radar

In principle, one could conceive of augmenting the long-wave infrared detection on board of high-flying airplanes or low orbit satellites by active illumination with a laser. (Lasers for search on the ground would be affected by the weather.) Because cryogenic cooling is not necessary, and detection is orders of magnitude more sensitive, one would in this case use photo-multipliers and visible or near-UV wavelength lasers. For point targets, the signal power P_r of such a laser radar (or lidar), received from a target at distance R, is given by the same equation (4-1) as was given for radar:

$$P_r = P_t \frac{G A \sigma}{(4\pi)^2 R^4} F_L. \qquad (4\text{-}38)$$

P_t denotes the laser power transmitted and A is the area of the receiving optics. The lidar cross section σ can be expressed using the reflectivity ρ and the area A_T of the target:

$$\sigma = 4 \rho A_T \qquad (4\text{-}39)$$

for a Lambertian reflector. The transmitting optics gain G is

$$G = \omega / 4\pi \qquad (4\text{-}40)$$

(ω is the beam solid angle), and will normally be kept markedly above the diffraction limited gain G_{DI}

$$G_{DI} = 4\pi A_t / \lambda^2 \qquad (4\text{-}41)$$

where A_t is the transmitting optics area, and λ the laser wavelength. The reason for this is the very small beam divergence possible with laser wavelengths (e.g., 10^{-12} steradian); without this artificial beam widening, more than 10^{10} beam positions would have to be searched, which would lead to unacceptably long search periods (frame times), taking into account that

the unambiguous pulse frequency for 500 km range is only 300 Hz. Even with strong beam widening, many thousands of positions would have to be searched, and frame times would amount to many seconds. This means that the backscattered signal for an approaching target increases strongly from frame time to frame time, and there will not be very many frame times after detection for the object to arrive. For these reasons, the cumulative probability of detection will equal the single-frame probability of detection. Therefore, and because a photo-multiplier is limited by its dark current (which can, for moderate cooling, be as low as 1 to 10 pulses of 1 nanosecond duration per second), the optimum signal-to-noise ratio will be achieved, if only one laser pulse of maximum energy is transmitted per search direction. The possibility of detecting single backscattered photons, distinguishes this detection scheme from the radar case, where the thermal noise in the antenna-receiver chain is the limiting factor. Since in the single-pulse detection scheme without averaging, light powers corresponding to a fraction of a photon cannot be detected, a limiting case for detection is the distance where one backscattered photon is expected per transmitted pulse. The lidar detection range could be defined as the distance from where 2 photons would be expected (using Poisson statistics for the dark current and signal pulses, for an ideal photon detector with quantum efficiency $\eta = 1$ and 10 dark pulses per second, setting the threshold at two or more pulses per 1 ns time interval leads to a false alarm probability of 10^{-16} and a detection probability of 0.59). Equating the product of (4-38) and of the measurement interval $\Delta t = 1/B$ (B: bandwidth) with $2 E_{Ph} = 2 h c / \lambda$, this detection range R_{Det} becomes

$$R_{Det} = \left[\frac{P_t A \sigma}{4 \pi \Omega F_L B} \frac{\lambda \eta(\lambda)}{2 h c} \right]^{1/4} \tag{4-42}$$

where $\eta(\lambda)$ is the quantum efficiency of the photo-multiplier at the lidar wavelength λ. Maximizing R_{Det} calls for the longest wavelength still detectable with a photomultiplier (i.e., about 0.6 μm). If one, as in Ref. 58 for the case of a uniformly searching radar, introduces the relations used for the derivation of (4-10), one can define a reference distance r_1 such that

$$R_{Det}^4 = r_1^3 \Delta, \tag{4-43}$$

where

$$r_1 = \left[\frac{P_{av} A \sigma}{4 \pi F_L \Omega v} \frac{\lambda \eta(\lambda)}{2 h c} \right]^{1/3}, \tag{4-44}$$

and Δ, the distance traveled by the approaching target during one frame time, can be chosen for optimized search detection range R_{DetS}. As in 4.1.1.3, v is the radial velocity of the target, P_{av} is the average power of the laser, and Ω is the solid angle to be searched. A solid criterion for Δ would be that one frame time after the first detection at R_{DetS} the target has not hit the lidar, but is still at, say, half the detection distance, i.e.,

$$\Delta = R_{DetS} / 2. \tag{4-45}$$

With this criterion, the optimum detection distance becomes

$$R_{DetS} = 0.5^{1/3} r_1 = 0.79 r_1. \tag{4-46}$$

What figures can be expected for the search detection range R_{DetS}? With a transportable high-energy laser, the average power could be $P_{av} = 1$ kW, the optics area $A = 0.79$ m^2, the wavelength $\lambda = 0.5$ μm. Let the lidar backscatter cross section of a reentry vehicle be σ =

0.2 m^2 (this is based on a reflectivity of $\rho = 0.2$ and an area of $A_T = 0.25\ m^2$), let the vehicle approach with a velocity of $v = 3$ km/s. With a search solid angle of $\Omega = 0.54$ steradian (90 and 20 degrees, respectively) and a loss factor of $F_L = 3$, the optimized search detection range becomes

$$R_{DetS} = 69\ km. \tag{4-47}$$

The optimum frame time is $T_f = 11$ s, the distance traveled in one T_f is $\Delta = 34$ km. With a pulse frequency of 1 kHz (pulse energy 1 Joule), the beam width becomes about 50 msr (0.2° half opening angle). This is no improvement at all over the search radius of a mobile radar. Significant increases neither in average laser power nor in optics diameter seem possible for systems which can be carried on board aircraft or moderate-size surveillance satellites. (Of course, laser weapons would be larger – but these would not be used for the search function.)

The conclusion is that laser radars do not offer an advantage for the search function. If, on the other hand, the trajectory of a target is approximately known from other sensors, a laser radar with sharply focused beam can give sufficient reflected power from much larger distances, and can thus be an efficient means for measuring the exact distance and position as well as for tracking; possibly, it could also contribute to decoy discrimination.

4.2 Tracking, Guidance, and Fusing

4.2.1 Tracking

After a search system has detected and possibly identified incoming ballistic missiles or their reentry vehicles, the trajectories of the objects have to be measured. This is a necessary prerequisite for the prediction of the target area, for deciding whether the interceptor missiles from a specific location would be kinematically able of hitting the objects, and for allocating specific defense systems to the targets. A special function is the trajectory measurement during interception in order to guide interceptors. This task is more difficult during reentry, because depending on the ballistic coefficient and the angle of attack of the warhead, the phase of maximum deceleration may happen at different altitudes. As derived in 4.1.1.3, because of the small solid angle involved, radars have a much greater range in the tracking, than in the search mode. Because of the shorter ranges involved and the higher angular resolution needed, tracking radars normally use shorter wavelengths and less power than search radars. Classical air and ballistic missile defense systems had a separate radar each for search, warhead tracking, interceptor tracking, and interceptor guidance. Modern phased-array radars provide the beam to be rapidly switched between these different functions, and have only one main radar system. In this case, a compromise must be made on the wavelength.

4.2.2 Guidance

Guidance has to know the locations and the velocity vectors of both warhead and interceptor, and has to compute a prediction of the further trajectories of both. According to the difference between this prediction and the intended conditions of interception, corrections to the interceptor trajectory have to be calculated, and then effected. This process has to be repeated continuously. Basic guidance up to a pre-determined point could also be executed

using an inertial navigation system. At least in the last phase, the position of the incoming vehicle has to be taken into account; here an external measuring device with a communication link to the missile, or a measurement system on board the interceptor is required.

Guidance has been successful if both trajectories intersect (or come near each other) in space, and at some point in time both objects are at a sufficiently small relative distance which allows the effect of the interceptor weapon to damage the warhead. Guiding nuclear interceptors to sufficiently low distances from the warheads (several tens of meters in the atmosphere, several km in space, see 4.3.4) is possible with a ground-based radar. For the higher accuracy required for conventional interception, tracking via the missile can be used: the ground-based radar still illuminates the target, but here the receiver is located on the missile, thus the finite error of the direction to the warhead results in a decreasing error of relative location, as the distance between both decreases. This scheme is used with the U.S. Patriot air defense missile: in order to make use of larger computer power, the Patriot missile relays its received radar signals down to, and receives guidance signals back from its ground station. In principle, an autonomous radar system located on interceptors could perform tracking by itself, as well as computing the guidance signals. This would require a larger power supply and computer size on board, and is thus only used for the very last phase of guidance, the terminal phase, when the warhead is already in the vicinity of the interceptor.

Infrared detection during the terminal phase of interception within the atmosphere is of doubtful utility, because before the deceleration phase the reentry vehicles are at about room temperature. This would require, on the one hand, cryogenic cooling of the detectors. On the other hand, fast movement of the interceptor missiles through denser atmospheric layers will have heated the infrared windows due to air friction. Whereas engineering solutions to these problems may be found, they will tend to be complex and costly. Therefore, within the atmosphere, millimeter-wave radar is usually foreseen for homing guidance of ballistic missile interceptors. For interception in space, however, passive infrared detection against the low background is possible.

To date, reentry vehicles are unguided and follow a ballistic trajectory (with one exception, the U.S. Pershing 2). A qualitatively new kind of difficulty would be introduced if the warheads were able to maneuver during reentry (be it in a random way to confuse a defense system, or controlled by some target recognition and terminal guidance system, as is used in the U.S. Pershing 2 missile). This could be done by aerodynamic flaps which deflect the warhead axis from the direction of the velocity vector and thus produce lift. Because there is a rough proportionality between lift and drag (for a given angle of attack), maneuvering capability would begin when the deceleration becomes significant (for altitudes of roughly 30 km and lower), would be maximum in the phase of highest deceleration, would then decrease again and persist at a lower level until impact or ignition (see 6.1.2.3).

Interceptor missiles could use flaps also, as long as they do not leave the lower atmosphere (again up to about 30 km). If targets are to be engaged above this altitude, the thrust vector of the main rocket engine could be controled, or additional thrusters pointing orthogonally to the axis could provide accelerations changing the direction of the interceptor velocity vector (this principle is used in the U.S. FLAGE ballistic missile interceptor and in the U.S. MHV anti-satellite vehicle)[59].

In space, infrared sensors could provide fairly large detection distances (see 4.1.3). Since on that scale (several tens to several hundreds of km), movement of unpowered objects is approximately along straight lines, with constant velocity, simple proportional navigation, where the angular rate of change of the interceptor velocity vector is proportional to the

measured rate of change of the angle to the target,[60] can provide a highly accurate hit (as was demonstrated in the U.S. Homing Overlay Experiment)[61]. Reentering warheads, on the other hand, experience strong decelerations, and a much more complicated guidance scheme, taking into account the course of the movement and a model of its behavior, will be required. If warheads were able to maneuver unpredictably, the task would become considerably more complex.

In principle, targets in space could be illuminated by laser beams, and the guidance on board the intercept vehicles could use simpler detectors without the need for cryogenic cooling. This would, however, make the process dependent on the continuing functioning of the light sources and their detectors, which on the other hand would betray their position. Therefore, the passive scheme is likely to be preferred for homing guidance.

4.2.3 Fusing

If and when the interceptor is sufficiently near the incoming warhead (normally some time before the minimum distance is actually achieved), the interceptor warhead must be triggered. The relative distance between both could be determined with little precision, sufficient for a nuclear interceptor, from a remote position, e.g., a ground-based radar. If higher accuracy is needed, as for conventional interceptors, some on-board distance sensing device is required. This could be the track-via-missile antenna with the link to the ground computer, the millimeter-wave radar used for terminal phase guidance, or a specific proximity fuse (also using mm-wave radar, but working over smaller distances with less power only). Proximity fuses are used routinely with air defense projectiles, they can have ranges of several hundred meters for aircraft.[62] For the faster and less reflecting reentry vehicles, some modification of the system may be necessary.

Infrared-guided direct-hit interceptors in space can do without any fusing mechanism, if they are sufficiently accurate to destroy their targets by their impact.

4.3 Interception Techniques

Techniques for interception of incoming reentry vehicles or missiles could be grouped in different ways. Here, at first the non-nuclear effects are dealt with, among them the exotic beam weapons techniques, then nuclear interception is analyzed. Interception could be effected by actual destruction of the warhead ("warhead kill" – this is particularly difficult for nuclear warheads), or by pushing the warhead out of its intended trajectory so that it misses its target by a safe distance ("mission kill"). Because interception by the overpressure shock wave is only relevant with nuclear interceptors, it is described under that heading. Damage radii of the different techniques are summarized in Table 4-6 at the end of 4.3.4.3.

4.3.1 Interception by Conventional Fragmentation Warhead

In free air, fragments are more effective as damaging mechanism than is the overpressure wave of a conventional explosion. Fragments are produced when the overpressure from the explosion breaks up the metal surroundings; sometimes prefabricated metal fragments are used. These fragments are accelerated by the expanding gases and spread isotropically, more or less forming a spherical surface. Their initial velocity v_F is given by [63]

$$v_F = c_G \left[\frac{m_{Ex}/m_M}{1 + a\, m_{Ex}/m_M} \right]^{1/2}, \qquad (4\text{-}48)$$

where m_{Ex} is the mass of the explosive, and m_M is the total metal mass converted to fragments. The Gurney constant c_G varies for the different explosives between 2.3 and 3.1 km/s; the shape factor a is 1/2 for a long cylinder, 3/5 for a sphere.[64] A spherical shape with c_G = 3 km/s, having equal explosive and metal masses results in an initial fragment velocity of v_F = 2.4 km/s; if 90% of the warhead mass is metal, the velocity decreases to v_F = 1 km/s. Although the fragments will have irregular shapes and high drag coefficients ($c_D \cong 2$), calculations show that steel fragments will not lose more than 1/3 of their velocity over a 50 m path in air at sea level.[65] Because ballistic missile interception takes place at reduced air density, and path lengths above 20 m are unrealistic (see below), for a rough estimate one can neglect drag on the fragments. The relative velocity, and incidence angle, of a fragment versus an incoming missile or reentry vehicle, depends in a complicated way on the velocity vectors of the incoming and intercepting missiles, and on those of the fragments relative to the center of gravity, as well as on the geometry and timing of the interception. In an estimate favoring the defense, one can postulate that the fragment and the reentry vehicle meet head-on, i.e., their velocities have to be added. This gives relative velocities of about 3, 5, or 8 km/s for missiles with ranges of 100, 1,000, or 5,000 km, respectively. These velocities are sufficient for penetration of light armor, if the fragment masses are sufficiently high. (For example, steel spheres of 4 – 6 mm diameter and 1 km/s velocity can easily penetrate 1.5 mm of steel.[66]) For reentry vehicles, 1 or 2 cm of thermal protective coating would have to be penetrated at first. Damage to the warhead could occur, if a fragment hit a fuse mechanism, or would penetrate a further metal casing to the conventional explosive of the incoming warhead. This will require greater fragment weights than are used against aircraft (maybe several 10 grams instead of several grams). In order to make an estimate of the damage radius which is optimistic for the defense, I assume that the reentry vehicle or missile presents its maximum projected area for fragment hits, i.e., about 0.5 m^2 for a reentry vehicle (cone of 1.5 m length and 0.6 m diameter) or about 4 m^2 for a short-range missile (cylinder of 6 m length and 0.6 m diameter; in case of larger multi-stage missiles, the first stages would have been separated already). Let us further assume that damage extends to a distance where at least one fragment hits the object area A on average. From even distribution of N_F fragments on a spherical surface, the radius for one average hit is

$$r_1 = \left(\frac{N_F A}{4\pi} \right)^{1/2}. \qquad (4\text{-}49)$$

Here the number of fragments N_F is given by the mean fragment mass m_F and the total metal mass m_M:

$$N_F = m_M / m_F. \qquad (4\text{-}50)$$

A typical payload of an anti-tactical ballistic missile interceptor could be 100 or 200 kg. With a total metal mass of m_M = 50 kg and a fragment mass of m_F = 50 g, N_F = 1,000 fragments are produced. Against a reentry vehicle (A = 0.5 m^2), the radius for one average hit becomes r_1 = 6 m. With a 200 kg warhead of which 80% is metal, N_F = 1,600 fragments of 100 g each are possible – this gives a damage radius of r_1 = 8 m. Against an entire missile, these radii increase to about 20 m; but, since passage of fragments through a burnt-out solid rocket motor, which makes up the most part of the missile area, will not stop the missile nor

prevent its fuse and warhead from working, this may only be the radius for mission kill. In order to achieve greater damage radii, fragment warheads with a certain amount of directivity could be developed.[67] This effect is limited for several reasons: use of a "shot-gun" type barrel would subtract from the fragment mass; mechanisms for aligning the fragment direction during the last split second would be complicated and would reduce fragment load, too; guidance reqirements increase as the fragment expansion cone gets narrower. Therefore, the increase of the damage radii and the corresponding decrease in guidance accuracy will probably not exceed a factor of 2 or 4. It may be instructive to compare these values to anti-aircraft defense: Here the projected area (e.g., seen from below) could be $A = 20\ m^2$; fragments of $m_f = 5$ g may suffice to penetrate the sheet metal of aircraft wings or fuselage. With $m_M = 50$ kg total fragment mass and a resulting total number of $N_F = 10{,}000$ fragments, the radius for one average hit becomes 130 m (however, several hits will be necessary for severe damage, reducing the damage radius to perhaps 30 to 50 m).

In sum, damage to incoming tactical ballistic missiles or their reentry vehicles by conventional fragmentation warheads, is only possible up to distances of no more than about 10 m. For reliable destruction of the fuse or the explosive, even smaller distances have to be achieved. Damage radii for deflection from the trajectory are about 10 m for reentry vehicles, and about 20 m for short-range ballistic missiles. If the incoming warhead carries a nuclear explosive, it may be salvage-fused if hits by fragments are sensed (see 6.1.2.7).

4.3.2 Interception by Direct Hit

If a reentry vehicle or missile hits a massive object, the former can be totally destroyed. If both objects meet with opposite velocity vectors, the relative impact velocity is between 2 and 7 km/s; if both velocities are perpendicular, impact is with 1 to 6 km/s. In most cases, the kinetic energy of the intercepting projectile will suffice to break up the reentry vehicle casing and to destroy the interior. (A 20 kg mass with 5 km/s velocity has 250 MJ kinetic energy, sufficient for full vaporization of 20 kg aluminum or 4 kg graphite.) Of course, a direct hit is required; with the typical size of a reentry vehicle, an accuracy of guidance and timing of 0.3 to 0.5 m is necessary. If such extreme accuracy can be provided, then the payload of the intercepting missile can be lowered from 50 to 200 kg (for a fragmentation warhead) to 10 to 20 kg.

In the vacuum of space without significant air drag, a precision-homing projectile may increase its effective damage radius by unfolding a net- or umbrella-like structure. In this way, damage radii of about 5 m may be achieved (as in the U.S. Homing Overlay Experiment)[68]. Munitions like this would have masses of 10 to 30 kg, and could be launched from the ground on top of relatively small rockets, or from satellites.

In principle, small projectiles could also be shot against ballistic missile reentry vehicles from electromagnetic guns. Research and development for electromagnetic acceleration of projectiles is part of the U.S. SDI program.[69] Because of high energy consumption, however, this does not seem to be efficient unless some form of terminal phase guidance could be implemented on board the projectile.[70] Overcoming the severe acceleration loads (of up to several 100,000 times the earth's gravity) requires considerable development effort. Whereas infrared seekers could at least conceptually be used on small projectiles in space, hit-to-destruction guidance in the atmosphere by millimeter wave radar seems impractical.

In conclusion, destruction of incoming reentry vehicles by direct hits of massive objects seems possible if the guidance system provides an accuracy of less than 0.5 m in the atmo-

sphere, or less than 5 m in space. If the reentry vehicle carries a nuclear warhead, salvage fusing will generally be possible (see 6.1.2.7).

4.3.3 Interception by Beam Weapons

4.3.3.1 Laser Weapons

In principle, missiles or reentry vehicles could be damaged or destroyed by focusing large amounts of laser energy onto them.[71] Damage mechanisms are, melting through a casing for irradiation over some time with high mean power, or mechanical shock from explosive ablation of the uppermost layer for very short pulses of extremely high power. (The nuclear-explosion pumped x-ray laser which would utilize the latter effect is treated in 4.3.4.3.) In both cases, a threshold fluence (energy per area) must be achieved which may be 200 MJ/m^2 for reasonably hardened missile bodies, and 1 or 2 GJ/m^2 for the thermally protected reentry vehicles of intercontinental missiles (this technique could easily be applied to shorter-range ballistic missiles).[72] A lower limit for the laser energy which has to be transmitted, can be derived from the assumption that beam spread by diffraction is the only process reducing the beam fluence (discarding all atmospheric effects). The maximum fluence H possible at a distance r from a laser beam of initial diameter D is given for constant amplitude and spherical (or plane) phase front at the transmitter; its value is

$$H = Q_L \frac{\pi D^2}{4 \lambda^2 r^2}, \tag{4-51}$$

where Q_L is the laser energy transmitted, and λ is the laser wavelength. In order to achieve a damaging fluence value H_{Dam} on the object, the required laser energy Q_{LDam} is then

$$Q_{LDam} = H_{Dam} \frac{4 \lambda^2 r^2}{\pi D^2}. \tag{4-52}$$

There has been some discussion on the use of ground-based mobile laser weapons against incoming reentry vehicles of tactical ballistic missiles in a terminal defense mode.[73] The laser type envisioned for this is the gas-dynamic CO_2 laser which is powered by a combustion process. (Electrical lasers have small efficiencies and are impractical for mobile systems, because their power systems would be to heavy; the only high power chemical laser useful in the atmosphere – the Deuterium Fluoride laser – uses the very expensive deuterium as a fuel, and would be significantly larger.) A mobile CO_2 laser with λ = 10.6 μm could permit a laser power of about 1 megawatt, and a beam mirror of maybe D = 1.5 m diameter. In order to damage a reentry vehicle at r = 10 km distance, then, after (4-52), with H_{Dam} = 1 GJ/m^2, a laser energy of Q_{LDam} = 6 MJ would have to be transmitted. This would take 6 seconds – whereas the reentry vehicle would take only about 4 seconds to arrive at the target, if it came from 1,000 km distance. If the irradiation started at r = 5 km distance, 1.6 MJ would be necessary which would take 1.6 seconds – about the same time the reentry vehicle would need to arrive. In principle, if the focus were continuously reduced as the distance to the vehicle decreased, at some short distance the damage fluence could be provided in less than the remaining flight time. This would, however, mean focusing the beam to less than 1 cm diameter and keeping this focus on the same spot of the reentry vehicle while it moves over several

dozen meters. If the vehicle is spinning (as is routinely done), this possibility is excluded, and the beam energy is distributed over a larger area.

Of course, this discussion is hypothetical. Keeping a beam focused on an object of 0.5 m size moving fast through a turbulent atmosphere at several kilometers distance is extremely difficult, near to impossible. In addition, atmospheric effects like absorption, scattering, thermal blooming etc. can severely hamper beam transmission. In case of precipitation or medium to strong cloud cover, transmission as a focused high-power beam can be totally prevented. Thus, the conclusion is that mobile laser weapons do not provide a realistic possibility for terminal-phase defense against tactical ballistic missiles. It may suffice for the destruction of airplanes or helicopters in fair weather, but the main effects may even be less – blinding of optical sensors.

These arguments would not hold for the kind of large space laser weapons that are envisioned by the U.S. SDI program. Here a fleet of fighting satellites would circle around the earth in orbits of about 1,000 km altitude. These could carry chemical lasers, or mirrors which focus the beams from ground-based free electron lasers (relayed via geostationary mirrors) on ballistic missiles.[74] Wavelengths could be shorter, allowing better focusing over large distances. Free electron lasers could inflict damage deep into the atmosphere (down to the clouds or even to the ground). If reliable discrimination of decoys from reentry vehicles were possible, the latter could also be attacked during the free flight phase. With a hardness of $H_{Dam} = 1\ GJ/m^2$, a typical distance of $r = 1{,}000$ km, a mirror diameter of $D = 10$ m, and a laser wavelength of $\lambda = 1\ \mu m$, after (4-52) a laser energy of $Q_{LDam} = 13$ MJ would be required. With a mean laser power of 50 MW (which is four orders of magnitude above present levels of free electron lasers), this would take 0.25 seconds. Adding to this a (very optimistic) slew time to the next target of 0.1 s, one laser – mirror-satellite combination could attack about 3 reentry vehicles per second. Short-range missiles with a range of 100 km would be accessible in altitudes above, say, 20 km, which translates to a possible engagement time of 2 minutes at most (see Table 3-1). A mass launch of more than 400 short-range missiles could not be covered by one such beam. For reentry vehicles of longer-range missiles, more time above the clouds is available, e.g., for 1,000 km range about 8 minutes. In this case, a mass launch exhausting one beam would require about 1,500 reentry vehicles – which might not be prohibitive, if these missiles were changed to carry three reentry vehicles each.

Because reentry vehicles are so hard to attack, because they cannnot confidently be distinguished from decoys, and because one missile may release several warheads, the main purpose of space laser weapons is to attack missiles during their boost phase. Here the targets are large, they are more vulnerable, and they betray their position by the large flame. With a hardness value of $H_{Dam} = 200\ MJ/m^2$, all other parameters being the same, one laser beam of 50 MW power could damage a missile body at $r = 1{,}000$ km distance within 0.05 seconds. Because of the finite slew time, however, the attack rate increases only to about 6 missiles per second. For intercontinental ballistic missiles, fast burn boosters are possible with only 50 seconds burn time.[75] The burn time of tactical ballistic missiles could be reduced to less than 40 seconds (which means less than 30 seconds above 20 km altitude). One laser-mirror combination could thus handle a mass attack of 200 missiles at most. Short-range missiles could be designed in such a way that they burn out at less than 20 km altitude (or at least switched to a sustainer burn with much reduced flame emission above 20 km) – thus attack during their boost phase can be made nearly impossible.

This discussion has neglected several technical difficulties. These include the problem of cloud cover above some of the ground-based laser sites, the necessity for active beam phase front control to overcome atmospheric fluctations, the problem of targeting the small missiles on top of the large flames etc. It is by no means clear that free electron laser beams of 50 MW mean power can be produced and directed over two times 40,000 km with focusing to less than 1 meter and slew times of less than 1 second. The main problem with space laser weapons, however, if they prove to be feasible and effective at all, will be the fact that the other side will also possess them (in addition to other kinds of space weaponry that both sides will command). In an attack scenario, the space weapons of both sides would probably not be much occupied by the respective tactical ballistic missiles, but by the threat from the mutual space weapons systems themselves. Comparing space laser weapons and ballistic missile in terms of efficiency alone is misleading; in addition, ways of creating holes in space weapons constellations have to be analyzed. For the present discussion, it suffices to note that no side could rely on the continued functioning of its space weapons in the event of crisis and conflict (for an assessment of mutual attack possibilities in space and of consequences for strategic stability, see Ref. 76).

Another fact deserves mentioning: warheads do not vanish if their carrier is damaged. Depending on the time after launch at which a missile is hit, the warheads may fly a shorter trajectory and still explode on the intended territory.[77] Laser attack against a nuclear warhead could be sensed and used to trigger the explosion (salvage fusing, see 6.1.2.7). Damaged warheads which did not explode could distribute radioactive material when reentering the atmosphere.[78]

4.3.3.2 Particle Beam Weapons

If high-power beams of high-energy particles could be produced and directed over large distances, they could provide the only mechanism for instantaneous internal damage capable of preventing salvage fusing of nuclear warheads, except a defense nuclear explosion itself. Because of interactions with the air (neutral particles are immediately ionized) and with the earth magnetic field (charged particles follow curved trajectories with radii of the order of 10 or 100 km), particle beam propagation within the atmosphere does not allow militarily useful distances (the self-focusing and self-guiding effects possible with electron beams do not provide long ranges in the low atmosphere)[79]. For propagation in the high atmosphere or in space, two kinds of particle beam weapons are possible: an electron beam traveling through an ionized channel produced by a laser beam, or a neutral particle beam.

A laser-guided electron beam would require a UV laser in the kilojoule pulse energy class. This laser would produce a channel of ionized molecules in the upper atmosphere; this effect would work at altitudes between 70 and 500 km.[80] Interactions with the positive charge of the ions would prevent the electron beam from spreading and from bending, but the electron pulse length would erode with distance. The electron energies would have to be tens of megaelectronvolt over distances of hundreds of km, and hundreds of MeV over thousands of km. Since for most materials the absorption length of 100 MeV electrons is [81]

$$L = \frac{1}{\rho k^*} \text{ where}$$

$$k^* = 0.02 \ldots 0.03 \text{ m}^2/\text{kg}, \qquad (4\text{-}53)$$

and ρ is the density, delivery of a dose of 1 MGy = 1 MJ/kg would require a beam energy of 0.2 to 10 MJ (with the primary energy requirement roughly ten times higher).

For the UV laser and the electron accelerator, a major research and development effort would be necessary. Scaling up above today's state of technology is necessary by one order of magnitude (i.e., a factor of ten) for the accelerator voltage; by two orders of magnitude for the pulse duration; by three orders of magnitude for the beam power; and by four orders of magnitude in distance traveled.[82]

A fundamental alternative would be to use neutral particle beams which would propagate in space on straight lines. Because even small amounts of gas would ionize the particles, after which they would move under the influence of the earth magnetic field, neutral particle beams cannot be used at altitudes below 100 km. Neutral particles can be formed by accelerating negative hydrogen ions and stripping off the excess electron in a gas cell. For an absorbed dose of 100 kJ/kg (more than sufficient to damage electronics, not capable of vaporizing material), pulse energies of 50 MJ on the target would be necessary. Beam pointing and beam divergence in the microradian range would have to be developed. Accelerator assemblies would have to be increased in voltage and duty cycle by two orders of magnitude each.[83]

In conclusion, particle beam weapons could, in principle, damage the interior of reentry vehicles or missiles in space. Because a large research and development program is needed even before a well-founded statement on technical feasibility could be made, and because many engineering problems can be foreseen concerning e.g. power supplies and reliability, it is extremely unlikely that particle beam weapons could be available within the next twenty years or so. If these weapons do, however, prove feasible and effective, then the remark made in connection with laser weapons in space applies: the military balance between two sides, and its degree of stability, should not be judged by comparing space weapons against ballistic missiles, but by the mutual attack capabilities of the space weapons systems themselves. Lastly, even if some nuclear warheads had been disabled, the problem of the radioactive material reentering the atmosphere would still persist.

4.3.4 Interception by Nuclear Explosions

This is the method used in the traditional anti-ballistic missile systems of the sixties and seventies. Within the atmosphere, in order to minimize collateral damages, explosive yields in the kiloton TNT range are used. Mechanical shock by the overpressure wave, or effects by the penetrating neutron and gamma rays can be used. In space, the x-rays from large (megaton TNT range) explosions can travel unhindered and provide a larger range than the other kinds of radiation. These x-rays are immediately absorbed in the upper layers of the reentry vehicles; explosive evaporation provides a mechanical shock which can disrupt the bomb mechanism.

4.3.4.1 Mechanical Shock by the Overpressure Wave Within the Atmosphere

When a missile warhead reenters the atmosphere, it experiences strong deceleration (with maximum values below 1,000 m/s^2). Whereas its mechanical structure must be able to withstand values like this, damage to the reentry vehicle or its internal components can occur if it experiences accelerations of several times 1,000 m/s^2.[84] (Note, however, that earth penetrating warheads are being developed which can withstand such high accelerations, see below.)

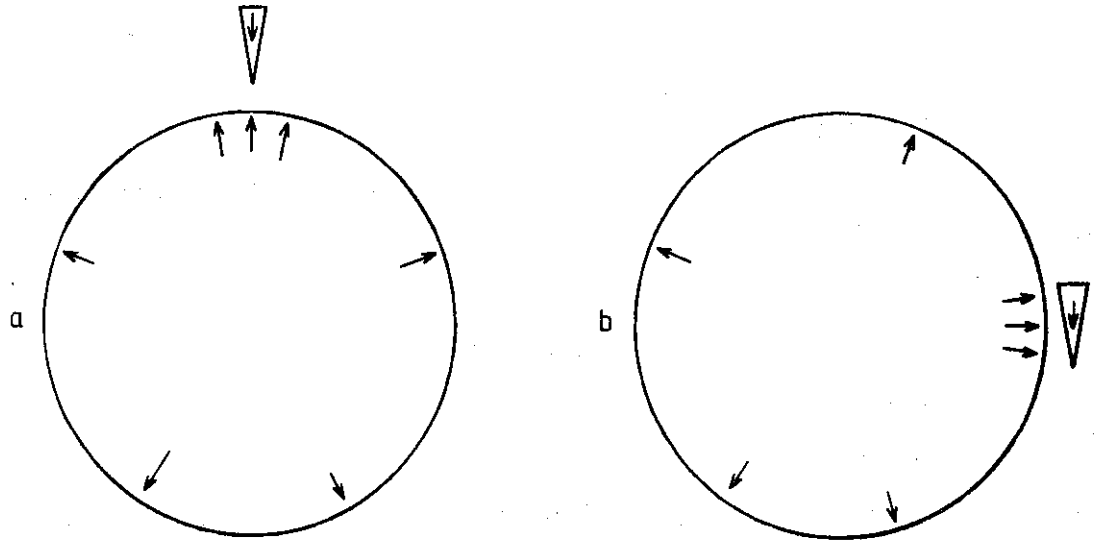

Fig. 4-12 Limiting cases of how a reentry vehicle and an explosion blast wave could collide.
a) Reentry vehicle velocity and particle velocity have to be added, low drag coefficient applies.
b) Particle velocity counts only, high drag coefficient applies.

The overpressure wave of an explosion in air can effect such an acceleration by two mechanisms: The peak overpressure produces a net force on the vehicle as long as it has not totally entered the blast wave. In the overpressure region of interest here, the dynamic pressure exerted by the outward-flowing air molecules is higher, and lasts considerably longer than the peak overpressure, therefore I will concentrate the analysis on the dynamic pressure. The increased air density in the shock wave enhances the preponderance of the dynamic pressure. Since the blast overpressures decrease rapidly with distance from the explosion center, damage to the reentry vehicle can only occur if the guidance system manages to ignite the interceptor warhead at such a time and at such a point, that the reentry vehicle hits the blast wave before it has expanded to a size where the dynamic pressure produces an acceleration below the damage value. Fig. 4-12 shows two limiting cases: in b), the reentry vehicle velocity is orthogonal to the particle velocity, and the dynamic pressure is only determined by the latter (see (4-54) below). In a), both velocities are opposed, and the dynamic pressure follows from the sum of the velocities (but, due to a lower drag coefficient, in this case the damage radius will be lower, see below).

For a quantitative estimation, we need the peak overpressure of a nuclear explosion in free air. This is given by [85]

$$\frac{\Delta p}{p_a} = 3.2 \cdot 10^6 \frac{1}{r_{sc}^3} \left[1 + \left(\frac{r_{sc}}{87}\right)^2\right]^{1/2} \left[1 + \frac{r_{sc}}{800}\right], \tag{4-54}$$

where the so-called scaled distance

$$r_{sc} = \left[\frac{\rho_a}{\rho_0} \frac{1\,\text{kt TNT}}{Y}\right]^{1/3} \left(\frac{r}{1\,m}\right) \tag{4-55}$$

contains correction factors for the ambient air density ρ_a at the explosion altitude, and for the explosive yield Y. (ρ_a and the ambient pressure p_a can be estimated from a simple exponential decrease from the sea level density ρ_0 and pressure p_0, respectively, with a scale height of 8 km.) Because the ambient pressure p_a and the density ρ_a are proportional to each other in case of constant temperature, in a first approximation the overpressures and damage radii are not dependent on altitude. The particle velocity u for a shock wave in air is given by [86]

$$u = \frac{5\,\Delta p}{7\,p_a}\,\frac{v_{Sound}}{(1 + 6\,\Delta p/(7\,p_a))^{1/2}}. \qquad (4\text{-}56)$$

Here $v_{Sound} = 340$ m/s is the sound velocity in the undisturbed air. The dynamic pressure experienced by the reentry vehicle is

$$p_d = 0.5\,\rho\,v_{eff}^2, \qquad (4\text{-}57)$$

where the increased air density ρ in the shock wave is [87]

$$\rho = \rho_a \frac{7 + 6\,\Delta p/p_a}{7 + \Delta p/p_a}, \qquad (4\text{-}58)$$

and the effective velocity v_{eff} is either equal to the sum of u and the reentry vehicle velocity v_{RV} (case a) of Fig. 4-12), or to the particle velocity u (case b) of Fig. 4-12). (For case b), the equation normally used for the dynamic pressure, (3-34), can be derived from (4-57).)

In order to estimate the damage radii, we need the relationship between the dynamic pressure p_d and the acceleration a, which can be derived from the air drag formula (3-2):

$$a = c_D\,p_d\,A/m = p_d/\beta. \qquad (4\text{-}59)$$

Here the ballistic coefficient β contains the drag coefficient c_D, the effective area A exposed to the pressure, and the mass m of the object. I take an acceleration of $a = 5{,}000$ m/s^2 (i.e., about 500 times the gravity acceleration) to be the threshold for damage to a traditional reentry vehicle. Let it be formed like a cone with 0.3 m radius and 1.5 m length, with a mass of $m = 150$ kg. Then, for case a), the area is $A = 0.3$ m^2, and the drag coefficient is about $c_D = 0.1$ (ballistic coefficient $\beta = 5{,}000$ kg/m^2). In this case, the damage pressure turns out to be 27 MPa. For a nuclear explosion of yield 1 kt TNT in free air, taking into account the reentry velocities (which, for 1,000 km range, decrease from 3 km/s to about 1 km/s), damage radii between 40 and 50 m result from (4-54) to (4-58). For case b), the area is $A = 0.5$ m^2, the drag coefficient is tenfold higher, about $c_D = 1$. Solving (4-59) for p_d, one gets a damage threshold value of dynamic pressure of $p_d = 1.7$ MPa. With a 1 kt TNT explosion in free air, such a dynamic pressure is achieved after (4-54) to (4-58) up to radii of about 80 meters.

The calculated damage radii can be decreased by increasing the ballistic coefficient (this is possible up to a factor of two in β), and by mechanically strengthening the reentry vehicle (in tests of earth-penetrating warheads, maximum accelerations of more than 7000 times the gravity acceleration have been measured)[88]. In this way, damage radii could be reduced by a factor of three, down to values of 10 to 30 m.

Thus, the conclusion is that nuclear interceptors of kiloton-range yields have damage radii by the blast overpressure against traditional reentry vehicles of 50 to 100 m; intense hardening of reentry vehicles can reduce these values, up to a point where radiation effects become dominant (see 4.3.4.2). Of course, the guidance and timing of the interceptor and warhead must provide an accuracy of comparable size.

4.3.4.2 Damage by Neutron and Gamma Radiation

A nuclear explosion produces neutron and gamma radiation in large amounts. Because these are the only effects which penetrate nearly instantaneously through the material of a reentry vehicle, they can be used if one tries to prevent a salvage fuse from working (see 6.1.2.7).

Neutrons can produce fissions in the fission trigger; if this produces sufficient heat, the trigger may lose its form or even ignite the chemical explosive. (Because one fission process releases about 200 MeV ($3.2 \cdot 10^{-11}$ J) energy, whereas one absorbed neutron releases at most its energy (for fission neutrons about 1 MeV), heating by direct absorption of neutrons in the fissile material is orders of magnitude less effective.) Gamma rays and neutrons can also be absorbed in the chemical explosive of the fission trigger; if it is heated above a certain temperature, ignition will occur. The radiation doses decrease with distance from the explosion because of geometric and absorption effects. The neutron fluence (i.e., the time-integrated number of neutrons per area N_n/A) at a distance r is approximately given by [89]

$$\frac{N_n}{A} = 1.9 \cdot 10^{17} \frac{1}{t\,TNT} \frac{Y}{r^2} e^{-(0.0042\ kg/m^4)\,\rho\,r}, \tag{4-60}$$

where the yield Y is in the kiloton range within, and in the megaton range outside of, the atmosphere. ρ is the air density. The corresponding neutron dose D_n in soft biological tissue (this should be similar to the dose in the chemical explosive) can be approximated by [90]

$$D_n = 4.7 \cdot 10^4 \frac{m^2\,Gy}{t\ TNT} \frac{Y}{r^2} e^{-(0.0042\ kg/m^4)\,\rho\,r}. \tag{4-61}$$

The gamma-ray dose D_γ in soft tissue can be approximated by [91]

$$D_\gamma = 6.5 \cdot 10^4 \frac{m^2\,Gy}{t\ TNT} \frac{Y}{r^2} f\,\alpha\, e^{-(m^3/kg)\,\rho\,r/\lambda}, \tag{4-62}$$

where the correction factors

$$\alpha = \frac{1 + 6\,(Y / Mt\,TNT)^2}{1 + 0.03\,(Y / Mt\,TNT)^2 + 0.005\,(Y / Mt\,TNT)^3}, \text{ and}$$

$$\lambda = (326 + 0.457\,(Y / Mt\,TNT)^2)\,m \tag{4-63}$$

account for reduced absorption through regions of reduced air density for megaton-size explosions, and f is the fission portion of the explosive yield (for three-stage hydrogen bombs, about 0.5). For kiloton-range explosions and in space, the correction factors are unity. For distances up to 100 m in air, and generally in space, the exponential absorption terms of (4-60) to (4-62) can also be ignored. ((4-61) and (4-62) give the dose values in Gray = J/kg; if the older unit rad is desired, note that 1 rad = 0.01 Gray.)

The thermal effects in both cases can be treated by the same formalism. Heating of a mass m by a temperature interval ΔT requires the energy input

$$Q = c_{mol}\,m\,\Delta T / m_{mol} \cong 3\,R\,m\,\Delta T / m_{mol} \tag{4-64}$$

(the molar specific heat c_{mol} is approximately three times the gas constant R = 8.31 J/(mol K), m_{mol} is the molar mass). The energy per mass, which for absorption equals the dose, is thus

$$Q / m = 3\,R\,\Delta T / m_{mol}. \tag{4-65}$$

If we assume that heating the chemical explosive or the plutonium-239/uranium-235 trigger material by a temperature interval of ΔT = 500 K is sufficient to ignite the explosive or otherwise disrupt the fission trigger, then for the explosive with $m_{mol} \cong 0.05$ kg/mol, the dose

for damage becomes $D = Q/m = 250$ kGy. For plutonium with $m_{mol} = 0.24$ kg/mol, the energy per mass becomes $Q/m = 52$ kGy. (If the possible use of insensitive high explosive had to be taken into account, a temperature interval of 1,000 K might even be required. In this case, the damage radii derived in the following would have to be divided by $\sqrt{2}$. In order to use an estimate which is optimistic for the defense, the lower temperature value is kept.) As mentioned, for the cases of interest here, all exponential and correction factors in (4-61) and (4-62) can be ignored. The sum of gamma and neutron doses to the explosive, as well as the neutron number per area, are then of the form

$$D = \text{const} \cdot Y / r^2, \tag{4-66}$$

and for a given damage dose D_{Dam} the distance r_{Dam} up to which this or a larger dose is delivered can be calculated from

$$r_{Dam} = (\text{const} \cdot Y / D_{Dam})^{1/2} \tag{4-67}$$

(i.e., damage radii obey square-root scaling with yield.) For gamma ray and neutron absorption in the explosive, this results in the following damage radii: for a 1 kt TNT pure fission ($f = 1$) explosion, $r_{Dam} = 21$ m. For a 1 kt neutron-enhanced warhead ($f = 0.5$, multiply (4-61) by an enhancement factor 10) $r_{Dam} = 45$ m. For a 1 Mt TNT hydrogen bomb ($f = 0.5$) in space, $r_{Dam} = 560$ m.

Now, the number of fissions produced shall be calculated. If σ_f is the fission cross section (for 1 MeV neutrons in ^{239}Pu, $\sigma_f = 1.80 \cdot 10^{-28}$ m^2, and in ^{235}U, $\sigma_f = 1.22 \cdot 10^{-28}$ m^2)[92], the number of fission processes N_f up to a depth l produced by an incoming neutron number N_n is given by

$$N_f = N_n (1 - e^{-(N_{Pu}/V)\,\sigma_f l}) \cong N_n (N_{Pu}/V)\,\sigma_f l \tag{4-68}$$

(here, the number density of plutonium atoms $N_{Pu}/V = N_L \rho_{Pu} / m_{mol}$, $N_L = 6.02 \cdot 10^{23}$/mole is Avogadro's number, $\rho_{Pu} = m/V = 19.5 \cdot 10^3$ kg/m^3 is the uncompressed plutonium density, $m_{mol} = 0.239$ kg/mol is its mole mass. The last approximation holds as long as the depth l is smaller than the mean free path $L = [(N_{Pu}/V)\,\sigma_f]^{-1} \cong 0.1$ m.) Let $Q_f = 3.2 \cdot 10^{-11}$ J be the mean energy produced by one fission process; taking into account that the volume is the product of beam (or material) cross section area A and depth l, the energy produced per mass can be deduced to be

$$\frac{Q}{m} = Q_f \frac{N_n}{A} \frac{N_L}{m_{mol}} \sigma_f. \tag{4-69}$$

Solving for the neutron number per area, and introducing the numbers given, one gets $N_n/A = 3.6 \cdot 10^{18}$/m^2 for the 500 K temperature increase. (This corresponds to a fissioned fraction of only $6 \cdot 10^{-10}$ of all nuclei.) This value is achieved for a 1 kt TNT fission weapon in a distance of $r_{Dam} = 7.3$ m, for a 1 kt enhanced radiation weapon at $r_{Dam} = 23$ m, and for a 1 Mt hydrogen bomb in space at $r_{Dam} = 230$ m.

In sum, nuclear explosions of the kiloton class can disrupt incoming nuclear warheads by internal thermal effects up to distances of 10 or 20 m; these damage distances can be increased by a factor of about 2 for enhanced radiation warheads. For megaton-size explosions in space, these kinds of damage extend to distances of 200 to 600 m.

4.3.4.3 Damage by Mechanical Shock from X-Ray Absorption

Within less than one microsecond after fission has begun, most of the energy of a nuclear explosion has been released, converting the bomb materials to a fireball of approximately $5 \cdot 10^7$ K temperature. At such temperatures, thermal radiation is in the form of x-rays, with peak wavelengths of about 0.1 nanometer (photon energies of about 10 kiloelectronvolt). The pulse of primary x-rays carries about 70% of the total energy released, spreads in space without absorption and blast effects, and lasts for several 100 nanoseconds only. X-rays of such energies are totally absorbed in a very thin layer of material (and cannot propagate through air). Because of the short duration, during the pulse no energy can flow to deeper layers. If the energy is much larger than the vaporization energy of the layer, this material will evaporate explosively, producing a recoil impulse on the remaining material. This mechanical shock can damage the casing or internal structures of missiles or reentry vehicles traveling through space. Since 1 kt TNT equals $4.2 \cdot 10^9$ J, the primary x-ray fluence H (energy per area) on an object at a distance r from a nuclear explosion of yield Y is

$$H = 2.9 \cdot 10^9 \frac{J}{t\,TNT} \frac{Y}{4\,\pi r^2}. \qquad (4\text{-}70)$$

If one assumes that the energy which has hit the surface is evenly distributed between kinetic and thermal energy of the vapour, then the impulse per area p/A can be derived to be [93]

$$p/A = 2\,(H\,\rho\,d)^{1/2} = 2\,(H/k)^{1/2}, \qquad (4\text{-}71)$$

where the inverse of the product of the density ρ and the absorption depth d is called the opacity k of the material. If the material is chosen to minimize x-ray damage (i.e., the atomic number chosen according to the x-ray wavelength), the threshold fluence H_{Dam} for producing a damaging value of the impulse per area $(p/A)_{Dam}$ is [94]

$$H_{Dam} = 250 \frac{MJ}{m^2} \left(\frac{(p/A)_{Dam}}{kPa\text{-}s}\right)^2 \left(\frac{E_{Ph}}{keV}\right)^{-3/2}, \qquad (4\text{-}72)$$

i.e., the damage fluence decreases with increasing photon energy E_{Ph}. For non-optimized material, H_{Dam} could be 5 times lower. A typical value of the damage impulse per area is $(p/A)_{Dam}$ = 2 kilopascal-second;[95] for photon energies of E_{Ph} = 10 keV and optimized material, the damage fluence becomes 30 MJ/m^2. In case of non-optimized material, it could decrease to 6 MJ/m^2.

The maximum distance r_{Dam} up to which this damage fluence is achieved, can be calculated from (4-70):

$$r_{dam} = \left[\frac{2.9 \cdot 10^9}{4\,\pi} \frac{J}{t\,TNT} \frac{Y}{H_{dam}}\right]^{1/2}. \qquad (4\text{-}73)$$

With a 1 Mt TNT explosion, this results in a damage radius of r_{Dam} = 2.7 km for optimized, and r_{Dam} = 6 km for non-optimized material.

In principle, much larger damage radii would be possible if a portion of the primary x-ray energy could be converted by a laser process to narrow beams; this requires, of course, that the accuracy of beam pointing is sufficiently high. Photon energies of such a nuclear-explo-

sion-pumped x-ray laser would be roughly a tenth of those of the pump photons, i.e., about 1 keV. If η_{tot} describes the portion of the total energy Q_{tot} released by the explosion which is converted to laser radiation, n is the number of beams pointing in different directions, and Ω_B is the solid angle of one beam, then the fluence H at a distance r is

$$H = \frac{\eta_{tot}\, Q_{tot}}{\Omega_B\, n\, r^2}. \qquad (4\text{-}74)$$

The damage radius r_{Dam} can then be calculated from the damage fluence H_{Dam}:

$$r_{dam} = \left[\frac{\eta_{tot}\, Q_{tot}}{\Omega_B\, n\, H_{Dam}}\right]^{1/2}. \qquad (4\text{-}75)$$

For a photon energy of E_{Ph} = 1 keV, the damage fluence after (4-72) is 1 GJ/m^2 for optimized material, and anywhere down to 200 MJ/m^2 for non-optimized material. With an explosive yield of Y = 100 kt TNT ($Q_{tot} = 4.2 \cdot 10^{14}$ J), a beam solid angle of $\Omega_B = 10^{-10}$ steradian, a beam number n = 4, and a total x-ray laser efficiency of $\eta_{tot} = 10^{-4}$, the damage radii become 300 km and 700 km, for the optimized and the non-optimized material, respectively. These figures are by no means reliable, because no values of achievable beam solid angle, beam number, or the laser efficiency are known.[96] In order to compensate for a small efficiency, the yield of the pump explosion could be increased up to about 10 megaton TNT; thus, it cannot be ruled out that damage radii of several times 1,000 km could be achieved, if nuclear-explosion pumped x-ray lasers become feasible at all, and are allowed to be fully developed.

In conclusion, missiles or reentry vehicles could be damaged by explosive x-ray ablation from megaton-size nuclear explosions in space at distances of several kilometers. If nuclear-explosion pumped x-ray lasers are feasible, they could have damage radii of several hundred km or even several 1000 km.

Table 4-6 summarizes the different interception mechanisms and their damage radii.

Tab. 4-6 Summary of damage radii of different interception techniques (excluding beam weapons). Interceptors have to be guided to less than these distances from the incoming missiles/reentry vehicles to be effective.

Interceptor mechanism	Damage radius	Remarks
Conventional fragmentation warhead	< 10 m	warhead kill
	20 m	mission kill
Direct hit	< 0.5 m	in air
	5 m	in space
Nuclear interceptor, kiloton size		
mechanical shock (blast wave)	10–100 m	in air
internal radiation damage	10–40 m	in air or space
Nuclear interceptor, megaton size		
mechanical shock (x-ray ablation)	3–6 km	in space
internal radiation damage	200–600 m	in space *)

*) Roughly the same figure would hold for air, but explosions of that size would not be used for missile defense in the atmosphere.

4.4 Data of Existing or Planned Anti-Tactical Ballistic Missile Systems

Table 4-7 shows the characteristics of selected radar systems which are or have been part of air or ballistic missile defense systems.

Table 4-8 lists the properties of long-range air defense missiles (i.e., with a range above 30 km) and of anti-ballistic interceptor missiles.

Properties of some interceptor missiles which are being developed in the U.S. Strategic Defense Initiative and are planned to be used against tactical ballistic missiles too, are given in Table 4-9.

Table 4-7 Properties of radar systems of selected air and ballistic missile defense systems.[97]

Hawk (USA)
Comprises four separate mechanically rotated radars:
Pulse Acquisition Radar PAR for aircraft detection at high- to medium altitudes, L band (1-2 GHz)
CW Acquisition Radar CWAR for aircraft detection at low altitudes
High Power Illuminator HPI for target acquisition and tracking, X band (8-12 GHz)
Range-Only Radar ROR for measuring range when the other radars cannot do so because of countermeasures, K band (18-27 GHz).

Patriot (USA)
Comprises one main phased-array radar for aircraft detection, and tracking (several smaller antennae for interceptor communication and guidance, identification friend or foe, and electronic countermeasures are mounted on the same flat face).

Designation:	AN/MPQ-53	
Frequency:	C band	(4-8 GHz)
Peak power:	100	kW
Average power:	10	kW
Antenna area:	4.68	m^2

Safeguard (USA)
Comprised two large fixed phased-array radars:
Perimeter Acquisition Radar PAR for Search and Detection:

Frequency:	442 MHz	(UHF band)
Peak power:	7.3	MW
No. of faces:	1	
Antenna area:	750	m^2
Search range:	4,000	km

(is now part of the NORAD early warning system)

Missile Site Radar MSR for tracking and interceptor guidance:

Frequency:	S band	(2-4 GHz)
Peak power:	1	MW
Average power:	100	kW
No. of faces:	4	
Antenna area:	13	m^2
Range:	1,000	km

(was deactivated in 1976)

Type	Country	First Deployment	Deployment Type	No. of Stages	Fuel Type	Max. Range, km	Max. Altitude, km	Burn Time, s	Acceleration, m/s^2	Velocity, km/s	Launch Mass, Mg	Total Length, m	Body Diameter, m	Payload, Mg	Warhead Type(s)	Nuclear Yield, kt TNT (conv. only; Warhead Mass, kg)	Guidance	Remarks
Air defense missiles with listed range above 30 km																		
Bloodhound	GB	1964	mobile	2	solid/ramjet	80	..	..	..	..	..	7.8	0.55	..	HE	..	semiactive	
Terrier	USA	1956	ship	2	solid	37	20	..	..	0.85	1.404	8.02	0.34	0.16	N,HE	1	semiactive	also surface-to-surface role
Hawk	USA	1960	mobile	1	solid	40	16	..	..	..	0.635	5.03	0.36	..	HE	75	semiactive	
Standard-2	USA	1978	ship	2	solid	55	20	..	..	0.85	1.360	7.99	0.34	..	N,HE	low kt	semiactive	also surface-to-surface role
Nike-Hercules	USA	1958	fixed	2	solid	140	45	..	..	1.1	4.858	12.65	0.80	0.51	N,HE	1-20	command	also surface-to-surface role; phased out.
Patriot	USA	1984	mobile	1	solid	100	25	12	300	1.2	0.912	5.31	0.41	..	HE	75	semiactive	track via missile; ATBM upgrading
SA-N-1	USSR	1961	ship	2	solid	31.5	..	..	..	..	0.40	6.6	0.70	..	HE	60	command	
SA-2	USSR	1958	mobile	2	solid/liquid	40-50	18	..	..	1.2	2.3	10.7	0.70	..	HE	130	command	also ship-born version: SA-N-2
SA-N-3	USSR	1967	ship	2	solid/ramjet	55	25	..	..	1.0	0.55	6.2	0.34	..	HE	80	semiactive	
SA-N-6	USSR	1978	ship	1	solid	55	..	..	..	1-2	..	7	..	..	HE	90	semiactive	track via missile
SA-4	USSR	1967	mobile	2	solid/ramjet	70	24	..	..	0.85	2.5	8.8	0.9	..	HE	135	semiactive	
SA-10	USSR	1980	mobile	1	solid	100	5?	..	..	2.0	1.5	7.0	0.45	..	HE	..	active	may have some A(T)BM potential
SA-12	USSR	–	mobile	1	solid	100	30	..	..	1.0	2.0	7.2	0.5	..	HE	150	active	may have some A(T)BM potential
SA-5	USSR	1967	mobile	2	solid	300	30	..	..	1.2	10	10.6	0.85	0.060	N,HE	..	..	
Anti-ballistic missile interceptors																		
Sprint	USA	1974	silo	2	solid	40	..	..	..	..	..	8.2	1.8	..	N	1	command	fast, for endoatmospheric intercepts, deactivated in 1976
Spartan	USA	1974	silo	3	solid	600	..	..	..	3.6	..	16.7	1.3	..	N	1000	command	deactivated in 1976
UR-96/ABM-1B	USSR	1964	fixed	3?	liquid	330	320	..	..	..	33	20	2.6	..	N	3000	command	for exoatmospheric intercepts
SH-04	USSR	1983	silo	..	..	..	..	..	..	..	..	..	..	..	N	..	..	modification of ABM-1B
SH-08	USSR	1984	silo	..	..	80	..	..	..	..	..	..	..	..	N	..	..	fast, for endoatmospheric intercepts

Table 4-9 Properties of selected systems and components planned to be used against tactical ballistic missiles.[98]

Interceptor missiles

Aster 30 (France)
2 stages; maximum range 35 km; course changes: aerodynamic plus lateral thrusters in terminal phase; guidance via multifunction radar, homing by active millimeter-wave radar.

FLAGE/ERINT (USA)
(Flexible Light-weight Agile Guided Experiment/Extended Range Interceptor) (formerly: SRHIT)
1 stage; length 3.7 m, diameter 0.23 m; launch mass 230 kg; burnout velocity 1.2 km/s; primary guidance for about 5 s by inertial unit; target acquisition by millimeter-wave radar, homing guidance for the last few seconds; course change by 216 lateral solid-rocket motors in front part of missile; damage to reentry vehicle by direct hit, guidance accuracy needed: 0.3 m; test intercepts for demonstration of guidance at about 4 km altitude and about 6 km range (e.g. May 21, 1987: a Lance short-range missile was intercepted at 3.7 km altitude; velocities were 0.98 km/s and less than 0.91 km/s for the FLAGE and the Lance, respectively).
The ERINT follow-on will have an additional stage, providing greater velocity; the radar seeker and the warhead will be modified; goal is interception of strategic ballistic missiles at 10 to 15 km altitude; tests planned for 1989-1990.

HEDI (USA)
(High Endoatmospheric Defense Interceptor)
2 or 3 stages; launch mass 5,000 to 7,000 kg; about Spartan size (ca. 15 m length); burn time 4 to 10 s; burnout velocity 5 to 6 km/s; primary guidance using signals of Terminal Imaging Radar (which is to discriminate decoys); after removal of shroud, homing guidance by short-wave infrared sensor looking through cooled window, acquisition at several dozen km; course changes by 12 liquid-fueled rocket engines; intercepts at 15 to 50 km altitude at up to 200 km range; damage to reentry vehicles by cloud of pellets, guidance accuracy needed: 1 m. Tests will begin in 1989 using modified Spartan first stage and Sprint first and second stages.

ERIS (USA)
(Exoatmospheric Reentry Interceptor System)
2 stages, goal: launch mass 700 kg; burnout velocity 5 to 6 km/s; interceptor mass 80 kg; guidance: inertial, terminal phase by long-wave infrared detector (goal: HgCdTe at T = 77 K); course change by liquid rocket engines; Intercepts at up to 1000 km altitude; damage by direct hit.
Homing Overlay Experiment HOE on June 10, 1984 used 1 t interceptor lifted by Minuteman I first stage and another stage, used unfolding umbrella-like structure.

Detection and Tracking Systems

AOS (USA)
(Airborne Optical System)
Long-wave infrared staring detector array: 38,400 elements on 15*4 chips of 10*64 each, doped Si, goal: HgCdTe; on board aircraft or unmanned RPV; gimballed optics with window, looking through air window in fuselage into space, for tracking of reentry vehicles during midcourse; payload 10-15 Mg; >12 h endurance, continous patrol at >15 km altitude. Flight tests against space objects using modified Boeing 767 to begin in 1989.

SSTS (USA)
(Space Surveillance and Tracking System)
Long-wave infrared detector array, carried on board satellites; for tracking of reentry vehicles and post-boost vehicles during post-boost and midcourse; later to be augmented by active discrimination.

Table 4-8 (previous page) Existing long-range air defense interceptor missiles and anti-ballistic interceptor missiles.[99]

Notes and References to Chapter 4:

1 See: M. I. Skolnik, Introduction to Radar Systems, New York etc.: McGraw-Hill, 1980, pp. 23–33.
2 Skolnik (note 1), Fig. 2.7, p. 28.
3 E. F. Knott, J. F. Schaeffer, M. T. Tuley, Radar Cross Section – Its Prediction, Measurement and Reduction, Dedham MA: Artech House, 1985, p. 178; J. N. Constant, Introduction to Defense Radar Systems Engineering, New York etc.: Spartan Books, 1972, p. 6-8.
4 For the MX missile (W87 warhead in Mk-21 reentry vehicle), the nose radius is 3.5 cm (1.4 in): T. B. Cochran, W. M. Arkin, M. M. Hoenig, Nuclear Weapons Databook, Vol. I, U.S. Nuclear Forces and Capabilities, Cambridge MA: Ballinger, 1984, p. 126.
5 Skolnik (note 1), p. 35-37.
6 Data calculations in the text and from tables and figures in: Skolnik (note 1), p. 44; Knott et al. (note 3).
7 Skolnik (note 1), pp. 46-52; P. Swerling, Probability of Detection for Fluctuating Targets, IRE Trans., vol. IT-6, pp. 269-308, April 1960.
8 Skolnik (note 1), p. 40.
9 Knott et al. (note 3), p. 421.
10 J. D. Mallett, L. E. Brennan, Cumulative Probability of Detection for Targets Approaching a Uniformly Scanning Search Radar, Proc. IEEE, vol. 51, pp. 596-601, April 1963, and vol. 52, pp. 708-709, June 1964.
11 M. I. Skolnik (Ed.), Radar Handbook, New York etc.: McGraw-Hill, 1970, p. 27-14.
12 Mallett/Brennan (note 10).
13 E. Brookner, Radar Technology, Dedham MA: Artech House, 1985, Ch. 3.
14 Mallett/Brennan (note 10).
15 D. C. Schleher, Introduction to Electronic Warfare, Dedham MA: Artech House, 1986, p. 210; Brookner (note 13), p. 25.
16 J. Clarke, Airborne Early Warning Radar, Proceedings of the IEEE, vol. 73, no. 2, pp. 312-324, February 1985.
17 Clarke (note 16).
18 Skolnik (note 1), pp. 330-331.; D. A. Boutacoff, Army Banks on Joint JSTARS for AirLand Battle Management, Defense Electronics, pp. 77-85, August 1986.
19 Skolnik (note 1), pp. 529-536.
20 See e.g.: K. J. Stein, Backscatter Radar Unit Enters Production Phase, Aviation Week & Space Technology, pp. 68-77, August 16, 1982; D. Hughes, Tests Verify OTH-B Radar's Ability to Detect Cruise Missiles, Aviation Week & Space Technology, pp. 60-65, March 21, 1988.
21 For an early review, see: W. C. Rochelle, Review of Thermal Radiation from Liquid and Solid Propellant Rocket Exhausts, NASA Technical Memorandum Y-53579, 1967. For more recent research, see e.g.: C. H. Gabbert, R. J. Hoffman, Reacting Multiphase Plume Characterization and Plume Effects: Including Gas-Particle Impingement Heating, AIAA Paper No. 70–845, AIAA 5th Thermophysics Conference, Los Angeles CA, June 29-July 1, 1970; S. M. Dash, D. E. Wolf, R. A. Beddini, H. S. Pergament, Analysis of Two-Phase Flow Processes in Rocket Exhaust Plumes, J. Spacecraft, vol. 22, no. 3, pp. 367-380, May-June 1985.
22 The spectral integration calculations of Sections 4.1.2 and 4.1.3 have been done using the program described in the Appendix.
23 R. Zirkind, Radiation from Rocket-Exhaust Plumes, Eleventh (International) Symposium on Combustion, August 14-20, 1966, Pittsburgh PA: The Combustion Institute, 1967, pp. 613-620.
24 These values are quoted as typical in: Science and Technology of Directed Energy Weapons, Report of the American Physical Society Study Group, Section 7.2.1, Reviews of Modern Physics, vol. 59, no. 3, pt. II, July 1987.
25 The American Physical Society Study Group on Directed Energy Weapons made a rough estimate using a blackbody model and arrived at 100 Megawatt infrared power for an ICBM: Science and Technology of Directed Energy Weapons, (note 24), Section 7.2.1.
26 This figure is given, for example, in the OTA report on ballistic missile defense: U.S. Congress, Office of Technology Assessment, Ballistic Missile Defense Technologies, OTA-ISC-254, Washington DC: U.S. Government Printing Office, September 1985, p. 159.
27 Cochran et al. (note 4), p. 116.
28 D. J. McCaa, Spectral Radiance Measurements of Exhaust Plumes from Scale Model Rocket Engines, Applied Optics, vol. 7, no. 5, pp. 899-903, May 1968.

29 W. L. Wolfe, G. J. Zissis (Eds.), The Infrared Handbook, Ann Arbor MI: Environmental Research Institute of Michigan, 1985, p. 3-53.
30 This formula can be understood if one assumes that the root-mean-square variation of the number of charge carriers is equal to the square root of the mean number of charge carriers produced in an integration time $\tau = 2 / B$. See also: W. G. Driscoll, W. Vaughan (Eds.), Handbook of Optics, New York etc.: McGraw-Hill, 1978, p. 8.
31 V. E. Zuev, Laser Beams in the Atmosphere, New York/London: Consultants Bureau, 1982, p. 340.
32 Zuev (note 31), p. 338-340.
33 R. A. McClatchey et al., Optical Properties of the Atmosphere, in: Driscoll/Vaughan (note 30), Ch. 14.
34 R. M. Measures, Laser Remote Sensing – Fundamentals and Applications, New York etc.: Wiley, 1984, p. 142.
35 McClatchey et al. (note 33).
36 Wolfe/Zissis (note 29), p. 3-34.
37 See e.g.: P. J. Klass, Early Warning Satellites Seen Operational, Aviation Week & Space Technology, pp. 18-20, Sept. 20, 1971; E. Ulsamer, Strategic Warning, Cornerstone of Deterrence, Air Force Magazine, pp. 40-47, May 1974. See also the remark on p. 4 in: Recent False Alerts from the Nation's Missile Attack Warning System, Report of Senator Gary Hart and Senator Barry Goldwater to the Committee on Armed Services, U.S. Senate, October 9, 1980, Washington DC: U.S. Government Printing Office, 1980.
38 R. M. Hord, CRC Handbook of Space Technology: Status and Projections, Boca Raton FL: CRC Press, 1985, pp. 141-147. See also: C. M. McCreight, Two-Dimensional Infrared Detector Arrays, Proceedings of the IAU Colloquium No. 79, Very Large Telescopes, their Instrumentation and Programs, Garching, April 9-12, 1984, pp. 585-602.
39 See e.g.: R. Neel, Challenges in processing data from mosaic sensors, in: W. S. Chan, J. T. Hall (Eds.), Mosaic Focal Plane Methodologies II, Proc. SPIE, vol. 311, p. 84-90, 1981.
40 Klass (note 37); B. G. Blair, Reconnaissance Satellites, pp. 125-133, in: B. Jasani (Ed.), Outer Space – A New Dimension of the Arms Race, London: Taylor & Francis, 1982.
41 Neel (note 39).
42 See e.g.: F. C. Gillett, M. W. Werner, SIRTF – The Next Step, NASA Technical Memorandum 86663, December 1984.
43 T. Limperis, J. Mudar, Detectors, Ch. 11 in: Wolfe/Zissis (note 29), p. 11-44.
44 Limperis/Mudar (note 43), p. 11-79.
45 Gillett/Werner (note 42).
46 D. E. Lencioni, W. E. Bicknell, D. L. Mooney, W. J. Scouler, Airborne measurements of infrared atmospheric radiance and sky noise, Proc. SPIE, vol. 280, pp. 77-88, 1981.
47 Lencioni et al. (note 46).
48 Gillett/Werner (note 42).
49 Lencioni et al. (note 46).
50 Lencioni et al. (note 46).
51 Lencioni et al. (note 46).
52 The optics size can be estimated from the photos in: D. Hobbs, An Illustrated Guide to Space Warfare, New York, Prentice Hall, 1986, p. 104-105.
53 Hobbs (note 52); Department of Defense Appropriations for 1987, Hearings before a Subcommittee of the Committee on Appropriations, House of Representatives, 99th Congress, Part 5, Research, Development Test and Evaluation, p. 667, Washington DC: U.S. Government Printing Office, 1986
54 G. H. Suits, Natural Sources, Ch. 3 in: Wolfe/Zissis (note 29), p. 3-19 – 3-40; R. Baker, L. W. Fredrick, Astronomy, 9th ed., New York etc.: Van Nostrand, 1971, pp. 328-329.
55 J. Miller, Lockheed U-2, Austin TX: Aerofax Inc., 1983, Ch. 9.
56 C. A. Robinson, Jr., Army Will Test Airborne Space Sensor, Aviation Week & Space Technology, pp. 47-51, July 2, 1984; Department of Defense Appropriations (note 53).
57 Report to the Congress on the Strategic Defense Initiative, Washington DC: Strategic Defense Initiative Organization, April 1987, pp. V-C-6 – V-D-4.
58 Mallett/Brennan (note 10).
59 J. D. Morocco, Army Missile Test Demonstrates FLAGE Guidance, Aviation Week & Space Technology, pp. 22-23, June 1, 1987; R. L. Garwin, K. Gottfried, D. L. Hafner, Antisatellite Weapons, Scientific American, vol. 250, no. 6, pp. 27-37, June 1984.
60 For a description of missile guidance schemes, see e.g.: P. Garnell, Guided Weapons Control Systems, London etc: Brassey's, 1980.

61 C. A. Robinson, Jr., BMD Homing Interceptor Destroys Reentry Vehicle, Aviation Week & Space Technology, pp. 19-20, 18 June 1984.
62 See e.g.: K. H. Wilke, Microwave Sensors for Intelligent Ammunitions, Military Technology, no. 5, pp. 32-42, May 1986.
63 G. F. Kinney, K. J. Graham, Explosive Shocks in Air, Berlin etc.: Springer, 1985, p. 27.
64 Kinney/Graham (note 63).
65 These calculations were done using the trajectory program described in the Appendix.
66 See e.g.: A. Weber, 76-mm-Kugelsplittermunition – Besonders zur Bekämpfung von Flugkörpern geeignet, Wehrtechnik, no. 4, pp. 98-101, April 1984.
67 See e.g.: M. Held, Die Wirksamkeit von Flugzielgefechtsköpfen, Internationale Wehrrevue, no. 3, pp. 343-347, March 1986.
68 Robinson (note 61).
69 Report to the Congress (note 57), pp. VI-D-5 – VI-D-8.
70 For discussions on the perspectives of electromagnetic weapons, see e.g.: A. Knoth, Electromagnetic Acceleration – a new ballistics?, Military Technology, pp. 18-22, June 1984; H. A. Bethe, R. L. Garwin, New BMD Technologies, Appendix A in: Weapons in Space, vol. II: Implications for Security, Daedalus, vol. 114, no. 3, Summer 1985.
71 See e.g.: J. Hecht, Beam Weapons – The Next Arms Race, New York/London: Plenum, 1984; S. Drell, P. J. Farley, D. Holloway: The Reagan Strategic Defense Initiative: A Technical, Political, and Arms Control Assessment, Stanford CA: Center for International Security and Arms Control, Stanford University, July 1984; Bethe/Garwin (note 70); J. Altmann, Laser Weapons – Dangers for Strategic Stability and Possibilities of Preventive Arms Limitation (in German), Marburg: Department of Physics, Philipps-Universität, 1986; Science and Technology (note 24); D. Schroeer, Directed-Energy Weapons and Strategic Defence, Adelphi Paper No. 221, London: International Institute for Strategic Studies, Summer 1987; G. R. Goldstein, The Requirements for Free Electron Laser Space Weapons: Possible of Prohibitive?, Report no. 18, Cambridge MA: Program in Science and Technology for International Security, Massachusetts Institute of Technology, November 1987.
72 Bethe/Garwin (note 70); Report of the Fletcher Commission, quoted in: C. A. Robinson, Jr., Study Urges Exploiting of Technology, Aviation Week & Space Technology, pp. 50-57, 24 October 1983.
73 G. Borm, The Military Utility of the Laser (in German), Wehrtechnik Nr. 12, pp. 73-76, December 1976; A. Knoth, EDI – A European Defence Initiative?, Military Technology, no. 12, pp. 18-26, December 1985; E. Heckmann, Air defence by means of high-energy lasers – Demonstration by MBB and Diehl, Military Technology, no. 1, pp. 60-62, January 1986; F.-W. Lindner, Laserwaffen für den taktischen Bereich, pp. 54-70, in: Jahrbuch der Wehrtechnik, Folge 16, Koblenz: Bernard & Graefe, 1986; K.-H. Allgaier, Die Abwehr der Luftraumbedrohung Europas, Wehrtechnik, no. 7, pp. 38-41, July 1986; France, Germany to Study ATBM Defenses for Own Needs, Aerospace Daily, p. 88, January 16, 1987.
74 Report to the Congress (note 57).
75 Bethe/Garwin (note 71).
76 Altmann (note 70), Chs. 4 and 5; J. Altmann, Offensive Capabilities of Space-Based Lasers, Bulletin of Peace Proposals, vol. 17, no.2, pp. 151-158, 1986; J. Altmann, Space Laser Weapons – Problems of Strategic Stability, to be published in: Bulletin of Peace Proposals, vol. 19, 1988.
77 For a calculation of this effect, see: P. D. Zimmerman, R. H. Howes, Collateral Damage Produced By Successful Defenses Against ICBMs: SDI Doesn't Solve the Problem, Physics and Society, vol. 16, no. 4, October 1987, pp. 9-11.
78 For first assessments of this problem see: Zimmerman/Howes (note 77); R. Howes, The Fate of Plutonium from Nuclear Warheads Destroyed by SDI, Paper given at American Physical Society Meeting, Crystal City VA, April 22, 1987.
79 G. Bekefi, B. T. Feld, J. Parmentola, K. Tsipis, Particle beam weapons – a technical assessment, Nature, vol. 284, no. 5753, pp. 219-225, March 20, 1980.
80 Science and Technology (note 24), Ch. 4.
81 Calculated after: Science and Technology (note 24), Section 4.2.3.
82 Science and Technology (note 24), Ch. 4.
83 Science and Technology (note 24), Ch. 4.
84 R. L. Garwin, H. A. Bethe, Anti-Ballistic Missile Systems, Scientific American, vol. 218, no. 3, March 1968, p. 21-31.
85 Kinney/Graham (note 63), p. 94.

86 S. Glasstone, P. J. Dolan, The Effects of Nuclear Weapons, Washington DC: U.S. Department of Defense and Energy Research and Development Administration, 1977, p. 97.
87 Glasstone/Dolan (note 86).
88 Earth Penetrating Weapons, Energy and Technology Review, June-July 1986, pp. 4-5.
89 Adapted from: H. L. Brode, Review of Nuclear Weapons Effects, Annual Review of Nuclear Science, vol. 18, 1968, pp. 153-202 (here: p. 176).
90 Adapted from Brode (note 89), p. 176.
91 Adapted from Brode (note 89), p. 177.
92 J. J. Schmidt, Neutron Cross Sections for Fast Reactor Materials, Part III: Graphs, KFK 120 (EANDC-E-35U), Karlsruhe, December 1962, pp. 206, 306.
93 Science and Technology (note 24), Section 6.3.5.
94 Adapted from: Science and Technology (note 24), Section 6.3.5. Note that the sign of the last exponent has to be negative, not positive as in the source.
95 Science and Technology (note 24), Section 6.3.5.
96 In his estimation, Ritson uses a typical value of 10^{-3} for the total efficiency: D. M. Ritson, A weapon for the twenty-first century, Nature, vol. 328, pp. 487-490, 6 August 1987.
97 D. Richardson, Patriot: A SAM for the '80s, Flight International, pp. 743-751, 5 September 1981; Le système d'arme mobile de défense aérienne Patriot, L'aeronautique et L'Astronautique, no. 101, pp. 56-72, 1983-4; B. Blake (Ed.), Jane's Weapons Systems 1987-88, London: Jane's, 1987 (and earlier years); Brookner (note 13).
98 Aster-30: J. M. Lenorovitz, Aerospatiale Studies Missile System To Counter Tactical Soviet Threat, Aviation Week & Space Technology (AWST), pp. 75-77, April 21, 1986; Mittlere und schwere Fla-FK-Systeme, Internationale Wehrrevue, no. 9, pp. 1455-1464, 1985;
FLAGE/ERINT: Army to Flight Test Nonnuclear ABM, AWST, pp. 30-31, January 24, 1983; LTV Missiles Group Wins Erint contract, AWST, p. 35, April 27, 1987; Report to the Congress on the Strategic Defense Initiative, Washington DC: Strategic Defense Initiative Organization, April 1988, pp. 4.2-20 – 4.2-22; Morocco (note 59);
HEDI: C. A. Robinson, Jr., Study Urges Exploiting of Technologies, AWST, pp. 50-57, October 24, 1983; C. A. Robinson, Jr., Panel Urges Boost-Phase Intercepts, AWST, pp. 50-61, December 5, 1983; Aerojet Receives $50 Million SDI Missile Subcontract, AWST, p. 27, April 28, 1986; Hughes Studies High Endoatmospheric Kill Vehicle, AWST, p. 101, May 26, 1986; High Endoatmospheric Defense Interceptor, AWST, pp. 75-77, November 23, 1987; Report to the Congress (loc. cit.), pp. 4.2-10 – 4.2-12;
ERIS: Robinson (note 61); C. A. Robinson, Jr., Panel Urges Boost-Phase Intercepts, AWST, pp. 50-61, December 5, 1983; Arms Control Reporter, no. 2, p. 575.B.202, 1987; Lockheed Developing ERIS Interceptor Vehicle, AWST, p. 73, March 16, 1987; Report to the Congress (loc. cit.), pp. 4.2-7 – 4.2-10; SDIO Forging Flight Test Plans For Controversial Weapons Concepts, AWST, pp. 57-61, November 23, 1987;
AOS: C. A. Robinson, Jr., Army Will Test Airborne Space Sensor, AWST, pp. 47-51, July 2, 1984; Department of Defense Appropriations for 1987, Hearings before a Subcommittee of the Committee on Appropriations, House of Representatives, Part 5, Research, Development, Test, and Evaluation, p. 667, Washington DC: U.S. Government Printing Office, 1986; J. T. Merrifield, Boeing Receives Flight Hardware for Airborne Optical Adjunct Tests, AWST, pp. 84-87, Nov. 10, 1986; Airborne Optical Adjunct, AWST, pp. 69-71, November 23, 1987; Report to the Congress (loc. cit.), pp. 4.1-12 – 4.1-16;
SSTS: Boost-Phase Requirements Lead Sensor Development Program, AWST, pp. 54-55, November 23, 1987; Report to the Congress (loc. cit.), pp. 4.1-9 – 4.1-10.
99 R. L. Garwin, H. Bethe, Anti-Ballistic Missile Systems, Scientific American, vol. 218, no. 3, pp. 21-31, March 1968; G. Rathjens, The Dynamics of the Arms Race, Scientific American, April 1969 (quoted in: J. N. Constant, Fundamentals of Strategic Weapons - Offense and Defense Systems, Part Two, pp. 78-79, The Hague etc.: Martinus Nijhoff, 1981); Constant, loc. cit.; Cochran et al. (note 4); J. M. Collins, U.S.-Soviet Military Balance 1980-1985, Washington etc: Pergamon-Brassey's, 1985; B. Wright, Soviet Missiles, Lexington: Heath, 1986; W. A. Smit, The Patriot Missile - an Arms Control Impact Analysis, pp. 156-176, in: F. Barnarby, M. ter Borg (Eds.), Emerging Technologies and Military Doctrine - A Political Assessment, Houndmills, London: Macmillan, 1986; Blake (note 97); U.S. Missiles, Soviet Missiles, Aviation Week & Space Technology, pp. 148-153, March 14, 1988; The Military Balance 1987-88, London: International Institute for Strategic Studies, 1987 (and earlier years); Soviet Military Power 1988, Washington DC: Department of Defense, 1988.